

Nowcasting SAF

**Retrieving Cloud Top Temperature and Height
in Semi-transparent and Fractional Cloudiness
using AVHRR**

Visiting scientist report – October 2001

Aarno Korpela

National Institute of Water and Atmospheric Research, New Zealand

Adam Dybbroe, Anke Thoss

Swedish Meteorological and Hydrological Institute

Nowcasting SAF

**Retrieving Cloud Top Temperature and Height
in Semi-transparent and Fractional Cloudiness
using AVHRR**

Visiting scientist report – October 2001

Aarno Korpela

National Institute of Water and Atmospheric Research, New Zealand

Adam Dybbroe, Anke Thoss

Swedish Meteorological and Hydrological Institute

Acknowledgements

The work described in this report was carried out at the Swedish Meteorological and Hydrological Institute (SMHI) by Aarno Korpela, in collaboration with Adam Dybbroe and Anke Thoss, during the period 31/8 - 17/11 2000, when Aarno was staying at SMHI. The visit was jointly funded by the EUMETSAT Satellite Application (SAF) framework and the New Zealand National Institute of Water and Atmospheric Research Ltd (NIWA), together with additional support from SMHI. We wish to thank all three organisations, and the people involved, for the arrangements of this visiting scientist study. We also wish to thank the forecasters at the Swedish airforce in Malmslätt, southern Sweden, and especially Tore Andreason, for collecting the cloud top height in situ reports used in the validation effort presented in this report.

Cover image

The cover image is an example illustrating the rationale for this work. Retrieving the cloud top temperature and height from satellite imagery becomes a difficult problem when the image pixel has fractional cloud cover or the cloud is semi-transparent. The radiance signal is a mixture of the background radiation field below the cloud, and emission from the cloud itself. Therefore, obtaining the cloud top temperature from the brightness temperature measurements requires a correction method in affected pixels. The cover image is based on cloud classification done for NOAA14 AVHRR data from the satellite pass at 24-Sep-2000 1434 UTC. Cloud top temperature in opaque cloud pixels, where the temperature can be determined from uncorrected radiances, are shown in blue colours. The remaining cloudy pixels, which do require the correction, are shown in red.

Abstract

Cloud top temperature and height estimates obtained from AVHRR infrared imagery require a correction for semi-transparency when cirrus layers are present. In this work we investigated the possibility of using the 11 μm and 12 μm window channel brightness temperatures for the correction. We developed software which implements a method based on the work of Inoue (1985) and Derrien et al. (1988). In this method the cloud top temperature is derived for each small image segment by fitting a curve to a two-dimensional histogram of the segment, formed by using the brightness temperature $T(11\mu\text{m})$ and the brightness temperature difference $T(11\mu\text{m}) - T(12\mu\text{m})$. By extrapolating the model fit of the distribution to the opaque limit, a temperature estimate can be assigned to the semi-transparent cloud pixels, thereby replacing the measured brightness temperature which observes the combined background radiation and cloud emission. In this work, in addition to implementing data processing with the histogram based correction, we also developed a graphical user interface for testing the method, in order to provide a tool for the overall evaluation of the product.

Contents

1	Preface	4
2	Introduction	5
3	Method	6
3.1	$(T_4 - T_5)/T_4$ histograms	6
3.2	Least-squares fitting	8
3.3	Radiance ratioing algorithm	11
4	Implementation	13
4.1	Configuration	13
4.2	Processing	13
4.3	Graphical user interface	17
4.4	Radiance ratioing computations	18
5	$(T_4 - T_5)/T_4$ histograms - General performance	20
6	Validation	23
6.1	Data	23
6.1.1	Satellite data	23
6.1.2	Radiosondes	24
6.1.3	Ground based measurements	24
6.1.4	Manual reports from Swedish airforce flight missions	24
6.2	Comparison against opaque retrieval	25
6.2.1	14:46 UTC, September 2, 2000	26
6.2.2	13:28 UTC, September 23, 2000	29
6.3	Comparison against flight observations	34
6.4	Comparison against ground based measurements and radiosondes	38
7	Conclusion and recommendations	40
A	Software	42
A.1	ctth_config.py	42
A.2	ctth.py	43
A.3	cloudtop.py	43
A.4	cttsegment.py	44
A.5	radratio.py	44
A.6	C extensions in ctth_cmod.C	44
A.7	Fortran modules in ctth_fmod.F	46
A.8	radratio.F	47
A.9	Fortran subroutine packages	47

1 Preface

The main part of the work including development and testing of the cloud top temperature and height algorithm for semi-transparent clouds was carried out during the stay of Aarno Korpela at SMHI in the autumn 2000. But when he left SMHI after the planned two and a half month stay, the report was not completed and a few loose ends were left behind. We could have finished the report quickly with the material prepared at that time, but it seemed unsatisfactory to do so, since we thought the quality of the report could be raised substantially by finishing the loose ends in a proper way.

The remaining work was obviously more difficult when being separated on each hemisphere of the Earth, and while having other duties with higher priority. But with a few efforts in the early Northern hemisphere spring and again in autumn, we think the report has reached a level where it should be of interest to a wider audience. There is obviously much more development work that could be done to refine the algorithm, if resources are available. Especially the validation needs more work, and so does the development of useful quality flags for the final output.

2001-10-19

Adam Dybbroe
Norrköping, Sweden

Aarno Korpela
Wellington, New Zealand

2 Introduction

Retrieving accurate cloud top temperature and height (CTTH) estimates from satellite imagery is required for weather analysis and nowcasting. Those applications in which a CTTH product is needed include the height assignment of tropospheric winds from cloud tracking, cloud height analysis for aviation forecasting, and the early warning of thunderstorm development.

For optically thick clouds the cloud top temperature estimate can be obtained directly from AVHRR infrared imagery. In this thick cloud case the top of the atmosphere radiation measured by the satellite sensor in a window or a near-window channel is close to the black body radiation of an object at the temperature prevailing at the cloud top level. Using a collocated model background temperature profile at the cloud location and a forward radiative transfer model for the path above the cloud, it is, in principle, possible to retrieve an accurate cloud top height and temperature estimate by comparing the computed and observed radiances. If, however, the cloud is semi-transparent, e.g. a thin cirrus layer high in the atmosphere, the radiance signal is a mixture of two components, partly absorbed background radiation and cloud layer emission component. In these cases the brightness temperature obtained from the radiance does not indicate the true cloud top temperature, but gives a warmer signal, giving a misleading cloud top height estimate. As a large part of cloudy areas may include semi-transparent cloud layers, it becomes important to have a method to account for the semitransparency effect, thereby obtaining more reliable cloud top temperature and height estimates with a high spatial coverage. Theoretically the semi-transparency correction is a challenging task, as the basic imagery lacks the direct information on a fundamental parameter, the cloud emissivity.

In the work presented in this report we implement a histogram correction method for AVHRR near infrared window channel brightness temperatures, based on the work of Inoue (1985) and Derrien et al. (1988). In this method the cloud top temperature is derived for each small image segment by fitting and extrapolating a curve to a two-dimensional histogram obtained from the $T(11\mu m)$ brightness temperature and the brightness temperature difference $T(11\mu m) - T(12\mu m)$ of the segment pixels.

3 Method

3.1 $(T_4 - T_5)/T_4$ histograms

In order to derive the theoretical expression for the observed arc like structure in a two-channel histogram as shown in figure 1 consider a radiance measurement in a channel at frequency ν_i .

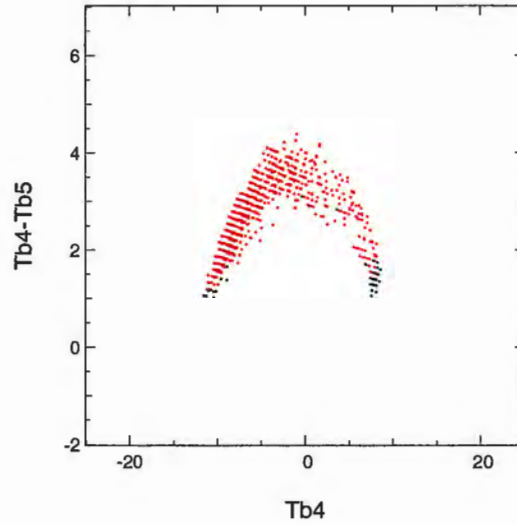


Figure 1: Example distribution of pixels from a 32x32 size image segment. Brightness temperature difference in AVHRR channels 4 ($11\mu\text{m}$) and 5 ($12\mu\text{m}$) is shown as a function of brightness temperature at channel 4. The pixels classified as clear are shown in blue, and the cloudy pixels are shown in red (semi-transparent) and black (opaque).

If a cloud layer of thickness z has absorption coefficient α_i which is constant throughout the layer, then the transmittance σ_i of a path at angle θ to vertical is given by

$$\sigma_i = \exp(-\alpha_i z / \cos \theta). \quad (1)$$

Transmittancies in two different wavelengths can be related as follows.

$$\begin{aligned} \ln \sigma_i &= -\alpha_i z / \cos \theta \\ \Leftrightarrow \ln \sigma_i^{1/\alpha_i} &= -z / \cos \theta \\ \Rightarrow \sigma_j^{1/\alpha_j} &= \sigma_i^{1/\alpha_i}, \end{aligned}$$

so that

$$\sigma_j = \sigma_i^{\alpha_j/\alpha_i}. \quad (2)$$

When the cloud-clear surface radiation intensity is $B_{s,i}$ below the layer, and when the semi-transparent cloud layer path has transmittance σ_i , emissivity ε_i and radiation intensity B_c at opaque limit, then in a window channel the measured radiance B_i at the top of the atmosphere is given by

$$B_i = \sigma_i B_{s,i} + \varepsilon_i B_c. \quad (3)$$

The opaque limit radiance B_c of the cloud does not depend on the frequency, because in a window or near-window channel there is no significant absorption above the cloud. At infrared frequencies the brightness temperature depends nearly linearly on the radiance, so that we may write the equation with the respective brightness temperatures as

$$T_i = \sigma_i T_{s,i} + \varepsilon_i T_c. \quad (4)$$

In local thermodynamical equilibrium (LTE) conditions we have the relation $\varepsilon_i = 1 - \sigma_i$, so that we can write the above equation as

$$T_i = T_c + \sigma_i (T_{s,i} - T_c), \quad (5)$$

or as

$$\sigma_i = \frac{T_i - T_c}{T_{s,i} - T_c}. \quad (6)$$

By applying the above equations (5) and (2) for AVHRR channels 4 and 5, and defining the ratio

$$\beta = \alpha_5 / \alpha_4, \quad (7)$$

we obtain for the difference $T_4 - T_5$ the expression

$$\begin{aligned} T_4 - T_5 &= T_c + \sigma_4 (T_{s,4} - T_c) - T_c - \sigma_5 (T_{s,5} - T_c) \\ &= \sigma_4 (T_{s,4} - T_c) - \sigma_4^\beta (T_{s,5} - T_c) \\ &= \sigma_4 (T_{s,4} - T_c) - \sigma_4^\beta (T_{s,4} - T_{s,4} + T_{s,5} - T_c), \end{aligned}$$

which by rearranging becomes

$$T_4 - T_5 = (\sigma_4 - \sigma_4^\beta) (T_{s,4} - T_c) - \sigma_4^\beta (T_{s,5} - T_{s,4}). \quad (8)$$

By equation (5) the measured brightness temperature T_4 changes from T_c to $T_{s,4}$ as the transmittance varies in the range of $[0, 1]$. In equation (8) the difference $T_4 - T_5$ plotted as a function of σ_4 forms an arc shaped curve opening downwards, the shape being determined by the ratio β . We see from the expression that on the left hand side of the curve, the 'opaque side', when $\sigma_4 \rightarrow 0$ and $T_4 \rightarrow T_c$, the difference vanishes. On the right hand side of the curve, the 'transparent side', when $\sigma_4 \rightarrow 1$ and $T_4 \rightarrow T_{s,4}$, the difference $T_4 - T_5 \rightarrow T_{s,4} - T_{s,5}$. This is the difference of the surface

brightness temperatures in the two channels, due to different absorption in the full path through the atmosphere and different emissivities of the surface in the two channels. In the case of AVHRR channels 4 and 5 the difference is of the order of 1K.

From a sample which has pixels with different transmittancies one can plot a $T_4 - T_5$ vs. T_4 histogram. Pixels with thick cloud show on the left hand side with $\sigma_4 \rightarrow 0$, and transparent pixels on the right hand side with $\sigma_4 \rightarrow 1$. Between these limiting values there are semi-transparent pixels from cirrus clouds, and possibly pixels with fractional cloud cover. In the case of cirrus, by fitting a curve to the arc structure of the histogram, one can determine the cloud top temperature T_c through extending the fitted curve on the left hand side to the point $T_4 - T_5 = 0$. If the difference $T_{s,4} - T_{s,5}$ estimate for the channels is computed with the forward model, then the surface brightness temperature $T_{s,4}$ can be found from the right hand side of the fitted curve.

Pixels with fractional cloud cover generally introduce a difficulty, when applying the two-window-channel histogram method. The cloudy fraction of the pixel contributes to a histogram location somewhere on the arc, while the clear fraction contributes to the end of the arc location on the right. Pixels with different cloud fractions and different transmittances then become distributed in the inner region of the arc, therefore making the model fit more inaccurate. On the other hand, differentiating fractional pixels from semi-transparent pixels during the cloud classification has uncertainty involved, so that part of the 'semi-transparent' pixels may actually be fractional, and vice versa. Therefore model fitting could be first tried with all pixels initially classified either way, and optionally only for pixels classified as semi-transparent.

3.2 Least-squares fitting

When we have the brightness temperature measurements $x_i = T_4$ and $y_i = T_4 - T_5$ from all pixels in a given segment we want to fit against these points the theoretical model (8), which by using the denotations $T_s = T_{s,4}$ and $\delta_s = T_{s,4} - T_{s,5}$ becomes

$$y(x, \mathbf{p}) = \left(\frac{x - T_c}{T_s - T_c} - \left[\frac{x - T_c}{T_s - T_c} \right]^\beta \right) (T_s - T_c) - \left[\frac{x - T_c}{T_s - T_c} \right]^\beta \delta_s. \quad (9)$$

where \mathbf{p} is a vector in a four-dimensional parameter space,

$$\mathbf{p} = (T_c, \beta, T_s, \delta_s).$$

One can test the agreement between the data and the model by choosing a *cost function*, which measures how much the points differ from the model,

and by minimizing it with respect to the parameters. The cost function could be the sum of the vertical distances from the model

$$S(\mathbf{p}) = \sum_{i=1}^N |y_i - y(x_i; \mathbf{p})|,$$

or the familiar sum of the squared distances,

$$S(\mathbf{p}) = \sum_{i=1}^N [y_i - y(x_i; \mathbf{p})]^2.$$

Theoretically one would like to answer the question "What are the most likely parameter values given the observed distribution?". First assume that at each point x the measurement has an independent random measurement error which has a normal distribution around the true model value $y(x; \mathbf{p})$, and that these error distributions have some common standard deviation σ . Then it follows that the maximum likelihood estimate is obtained by minimizing the least-squares expression

$$S(\mathbf{p}) = \sum_{i=1}^N [y_i - y(x_i; \mathbf{p})]^2. \quad (10)$$

When the dependent variable y_i has varying standard deviation σ_i , then the maximum likelihood estimate is obtained by minimizing the *chi-square* expression

$$\chi^2(\mathbf{p}) = \sum_{i=1}^N \left(\frac{y_i - y(x_i; \mathbf{p})}{\sigma_i} \right)^2. \quad (11)$$

When the model depends linearly on the parameters, i.e. when the parameters are the coefficients of some basis functions, the maximum likelihood estimate can be solved analytically from equation (11). Further, in this linear case the probability Q that the value of χ^2 exceeds a given value x can be computed from the formula,

$$Q(n, x) = \frac{\Gamma(n/2, x/2)}{\Gamma(n/2)} = \frac{\int_{x/2}^{\infty} e^{-t} t^{n/2-1} dt}{\int_0^{\infty} e^{-t} t^{n/2-1} dt}, \quad (12)$$

(Press et al. (1986)), where n is the number of degrees of freedom, $n = N - M$, when M is the number of model parameters. When the model depends nonlinearly on the parameters, as is the case with the histogram model (9), the minimization of the χ^2 function must be done iteratively, starting from a first guess set of parameters. In this general minimization problem a straightforward method is the *steepest descent method*, in which

the next point \mathbf{p}_{i+1} in the parameter space is found by minimizing the function along a line in the direction of the local downhill gradient at current point \mathbf{p}_i , so that

$$\mathbf{p}_{i+1} = \mathbf{p}_i - \text{constant} \cdot \nabla f(\mathbf{p}_i). \quad (13)$$

This is, however, a rather unefficient method, as the gradient in the new location has a vanishing component along the old direction, and therefore the gradient and the new direction must be perpendicular to the old direction, and generally this is not the best direction towards the minimum. In *variable metric methods*, which are also called *quasi-Newton methods*, the new direction is modified for this reason. Near the current point \mathbf{p}_i we have, to the second order

$$f(\mathbf{p}) = f(\mathbf{p}_i) + \nabla f(\mathbf{p}_i) \cdot (\mathbf{p} - \mathbf{p}_i) + (\mathbf{p} - \mathbf{p}_i) \cdot \mathbf{H} \cdot (\mathbf{p} - \mathbf{p}_i)^T,$$

where \mathbf{H} is the Hessian matrix of second derivatives. Taking the gradient gives

$$\nabla f(\mathbf{p}) = \nabla f(\mathbf{p}_i) + \mathbf{H} \cdot (\mathbf{p} - \mathbf{p}_i).$$

In Newton's method the step to the next iteration point is obtained by solving \mathbf{p}_{i+1} from $\nabla f(\mathbf{p}_{i+1}) = 0$, which gives

$$\mathbf{p}_{i+1} = \mathbf{p}_i - \mathbf{H}^{-1} \cdot \nabla f(\mathbf{p}_i). \quad (14)$$

The iteration method is termed quasi-Newton if an approximation \mathbf{H}_i of the Hessian is being used instead of the true Hessian. The probability of χ^2 exceeding a given value with a nonlinear model is no longer given by (12), but it is nonetheless usual to use this value as a relative measure for the goodness of fit.

In minimizing the chi-squared cost function (11) one needs its first and second derivatives, which are

$$\frac{\partial \chi^2}{\partial p_k} = \sum_{i=1}^N -\frac{2}{\sigma_i^2} [y_i - y(x_i; \mathbf{p})] \frac{\partial y(x_i; \mathbf{p})}{\partial p_k}$$

and

$$\frac{\partial^2 \chi^2}{\partial p_l \partial p_k} = \sum_{i=1}^N \frac{2}{\sigma_i^2} \left[\frac{\partial y(x_i; \mathbf{p})}{\partial p_l} \frac{\partial y(x_i; \mathbf{p})}{\partial p_k} - [y_i - y(x_i; \mathbf{p})] \frac{\partial^2 y(x_i; \mathbf{p})}{\partial p_l \partial p_k} \right].$$

With a good model the terms including the second derivative of the model tend to cancel out, as they are multiplied with the random measurement error $y_i - y(x_i; \mathbf{p})$. As they contribute negligibly to the sum they are usually ignored, so that the second derivatives of χ^2 are computed from

$$\frac{\partial^2 \chi^2}{\partial p_l \partial p_k} = \sum_{i=1}^N \frac{2}{\sigma_i^2} \left[\frac{\partial y(x_i; \mathbf{P})}{\partial p_l} \frac{\partial y(x_i; \mathbf{P})}{\partial p_k} \right].$$

At most this will affect the route taken to the minimum, not the minimum solution itself.

Among the different routines implementing the χ^2 minimization the *Levenberg-Marquardt method* has become the standard of least-squares fitting. It combines both the steepest descent and variable metric methods. In this work two different software packages were implemented for the minimization, one from the Numerical Recipes, and one from the Starpac statistical algorithm package. Both routines require the first derivatives of the model explicitly, rather than estimating them numerically. From (9) we obtain at a given point $(x_i, y(x_i))$ the expressions

$$\begin{aligned} \frac{\partial y}{\partial T_c} = & \frac{x_i - T_s}{(T_s - T_c)^2} \left(T_s - T_c + \beta \left[\frac{x_i - T_c}{T_s - T_c} \right]^{\beta-1} (\delta_s + T_c - T_s) \right) \\ & - \frac{x_i - T_c}{T_s - T_c} + \left[\frac{x_i - T_c}{T_s - T_c} \right]^\beta, \end{aligned} \quad (15)$$

$$\frac{\partial y}{\partial \beta} = (\delta_s + T_c - T_s) \left[\frac{x_i - T_c}{T_s - T_c} \right]^\beta \ln \left(\frac{x_i - T_c}{T_s - T_c} \right), \quad (16)$$

$$\begin{aligned} \frac{\partial y}{\partial T_s} = & \frac{T_c - x_i}{(T_s - T_c)^2} \left(T_s - T_c + \beta \left[\frac{x_i - T_c}{T_s - T_c} \right]^{\beta-1} (\delta_s + T_c - T_s) \right) \\ & + \frac{x_i - T_c}{T_s - T_c} + \left[\frac{x_i - T_c}{T_s - T_c} \right]^\beta, \end{aligned} \quad (17)$$

$$\frac{\partial y}{\partial \delta_s} = \left[\frac{x_i - T_c}{T_s - T_c} \right]^\beta \quad (18)$$

for the four derivatives. In the implementation we have provided these computations in subroutine modules, which can be called by the fitting algorithms.

3.3 Radiance ratioing algorithm

In this section we briefly describe the *radiance ratioing method* (Smith et al. (1974)) for deriving the cloud top pressure and height from sounding radiometer radiances (e.g. from HIRS). Collocating these radiances with AVHRR data provides one method for evaluating the heights obtained from the histogram method.

In a cloud clear case the measured top of the atmosphere radiance in a sounder channel can be written as

$$I_{cc} = B_s \sigma_s + \int_{p_s}^0 B(p) \frac{d\sigma_p}{dp} dp, \quad (19)$$

where B_s is the Planck radiance at surface temperature, σ_s is the surface to space transmittance, p_s is the surface pressure, $B(p)$ is the Planck radiance at pressure level p , and σ_p is the transmittance from level p to space. Similarly, the measured radiance from an opaque cloud at pressure level p_c is

$$I_{op} = B_c \sigma_c + \int_{p_c}^0 B(p) \frac{d\sigma_p}{dp} dp, \quad (20)$$

where B_c is the Planck radiance at cloud top temperature, σ_c is the cloud to space transmittance and p_c is the cloud top pressure.

We can next find the expression for the measured radiance in the case when the cloud is semi-transparent, having the emissivity ε , and under LTE the transmittance $\sigma = 1 - \varepsilon$.

$$\begin{aligned} I_{cl} &= (1 - \varepsilon) \left[B_s \sigma_s + \int_{p_s}^{p_c} B(p) \frac{d\sigma_p}{dp} dp \right] + \varepsilon B_c \sigma_c + \int_{p_c}^0 B(p) \frac{d\sigma_p}{dp} dp \\ &= (1 - \varepsilon) \left[B_s \sigma_s + \int_{p_s}^0 B(p) \frac{d\sigma_p}{dp} dp \right] + \varepsilon \left(B_c \sigma_c + \int_{p_c}^0 B(p) \frac{d\sigma_p}{dp} dp \right) \\ &= (1 - \varepsilon) I_{cc} + \varepsilon I_{op}. \end{aligned}$$

In a general case the FOV may have a cloud fraction N , in which case the measured radiance is given by

$$I = N I_{cl} + (1 - N) I_{cc}. \quad (21)$$

combining the last two equations gives

$$I - I_{cc} = N \varepsilon (I_{op} - I_{cc}). \quad (22)$$

Due to the height dependency in the opaque cloud radiance I_{op} measurements from two HIRS channels can be used to obtain the cloud height information. If the two channels have frequencies close to each other they have the ratio of the emissivities close to one, and we then obtain for channels m and n the relation

$$\frac{I_m - I_{cc,m}}{I_n - I_{cc,n}} = \frac{I_{op,m} - I_{cc,m}}{I_{op,n} - I_{cc,n}}. \quad (23)$$

This equation is the basis for the radiance ratioing method for deriving the cloud top pressure and height. By simulating the clear radiances and the opaque cloud radiances at different pressure levels one can find the level where the two ratios are closest to equal when the measured radiances are substituted. From the model background one can then get an estimate of the respective temperature and height of the cloud layer.

4 Implementation

The computing environment at SMHI for Nowcasting SAF development work included Python routines for reading the required input data, i.e. the AVHRR infrared channel data together with NWP model background data and the cloud type product files, so that building the CTTH prototype application with Python was the most straightforward approach. As most of the code has to do with preparing the data for the least-squares fitting algorithm, we could write that with the Python interpreter without losing too much of the computing speed, while benefiting from some of the Python prototyping features. Only the computationally expensive least-squares fitting routines and the respective interfaces were implemented using C- and Fortran extensions.

4.1 Configuration

The configuration settings which define the data sources and the computing method details are specified in a single configuration file *ctth_config.py*. The file is read in by the Python program modules.

CTTH processing requires four different source data files:

Physiography	land/sea mask for the area,
Preprocessed data	model background and RT computations,
AVHRR data	AVHRR channel 4 and channel 5 data,
Cloud data	cloud classification from AVHRR data.

These input files are in the hdf5 file format. Directory specifications for the input files are given in the configuration file for the ease of modifications. Any change in the name convention of these input files will require changes to the *loaddata* subroutine in the Python main module *ctth.py*.

Three additional directories are specified as well, which are not required in the main processing. These are the directory for HIRS data files used in the radiance ratioing method, the directory for radiosonde data files used in plotting the RS profiles, and the directory for Python program modules in CTTH implementation.

Processing options are specified through the various components of the global list *SETTINGS*. Appendix A shows an example configuration file, and we describe the different options in more detail in the following section.

4.2 Processing

The Python module *ctth.py* is the main program. It reads the configuration file, reads the input data files related to the processing request, and then

starts the processing. The processing request, which is the satellite pass time and the region of interest, is specified through command line arguments in the form

```
> ctth.py <yyyymmddhhmi> <area> <satellite>
```

for example as

```
> ctth.py 200009241343 cliwanet_north noaa14
```

Data specification from the arguments together with the directory names from the configuration file are used to locate the required input data files. During the processing the routine steps through the image area by segmenting it into image segments of specified size. Based on the cloud classification, the pixels in a given segment are provided to the model fitting routine if they are either cloud-clear, cirrus or fractional cloud pixels. For each image segment histogram fitting is done up to three times. If the segment is completely over land or completely over water, then only one fitting is required. When both land and water pixels are present, the fitting is done separately for both subsets, because the pixels will form two different arcs on the histogram, due to the different surface temperatures. Histograms in figure 2 show the "over-land" and "over-water" fits for one example segment located over the coast.

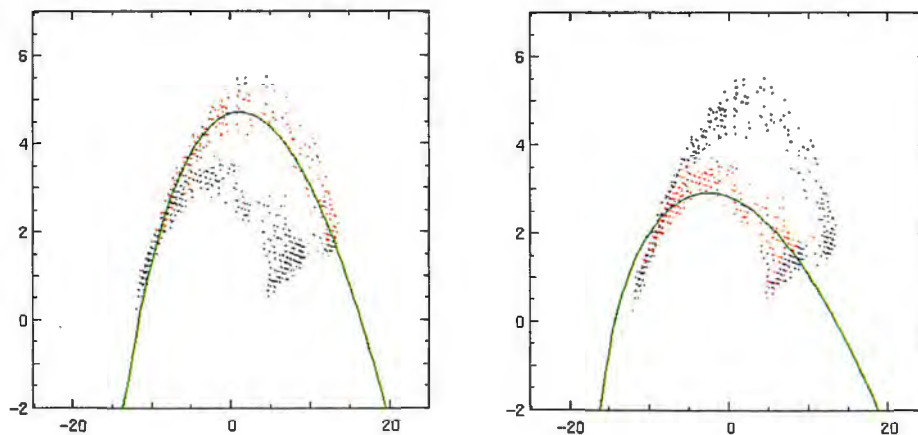


Figure 2: Model fitting done separately for the pixels over land (left) and for the pixels over water (right) in a single image segment histogram. The green points are clear pixels over land, the blue pixels are clear pixels over water, the red pixels are the target pixels for the temperature retrieval (either semi-transparent or fractional cloud pixels), and finally the black points are the excluded pixels in each case.

If both subsegments provide an estimate of the cloud top temperature, then the result for the segment may be computed e.g. by the weighted mean

of the two. If neither of the subsegments give a result, then a further third fitting is tried with all clear and target pixels included.

Due to the segmentation being done using fixed size segments in fixed positions (a grid of segments starting from the lower left corner of the image area) some segments by chance may contain a distribution in which the fitting fails, although nearby segments produce a result. To obtain as good a coverage as possible with acceptable results, the image area can be processed up to four times using a differently positioned segment grid. The number of segment locatings can be specified in the configuration settings, and the given number (1-4) of segmentations are made in the following order.

- 1 the default segmentation
- 2 shifted half-width right and half-height up
- 3 shifted half-width right
- 4 shifted half-height up

Obviously the the best coverage of succesful fits results from using all shifting modes, and the only reason to restrict this is the total computing time requirement.

As a result of the shifted segmentations the default segment is divided into four quarters or subsegments, and for each of them there could be up to four solutions from the four different segmentations. If there are both overland results and over-water results, then in principle the number of results for a given subsegment can be higher than four. In the current version the final solution for a subsegment is the weighted mean over all results, the weighting being done by using the number of target pixels in each fit.

We now go through the settings in the configuration file, as listed in Appendix A. The first two values set the default functioning and the level of output printing, respectively.

```
SETTINGS['runmode'] = "batch" # batch / xwindow
SETTINGS['verbose'] = 0       # Output print level 0,..,7,..
```

As mentioned already, the default run-mode is "batch", which does the least-squares fitting for all the image segments from the input data. The other possibility is the X-window mode for browsing results, as will be described later. Increasing the 'verbose' number will add more output printing throughout the processing. These two settings may also be changed with command line options, by specifying "batch" or "xwindow", and by giving some substring of "verbose" at the end of the command line.

The configuration settings that define the basic processing method are the following.

```

SETTINGS['lsqname'] = "starpac" # Lsq fit (python/numrec/starpac)
SETTINGS['nfree'] = 3          # No of free parameters (2-4)
SETTINGS['segw'] = 32         # Segment width
SETTINGS['segh'] = 32        # Segment height

```

Three different Levenberg-Marquardt method implementations are available for the 'lsqname' setting. "python" uses the method implemented in the Scientific python module. It is here for testing purposes only, as it is too slow for operational processing. "numrec" uses the method from Numerical Recipes, and the default, "starpac", uses the freeware statistical algorithm package *Starpac*.

The theoretical model for the arc shape histogram has four free parameters.

T_c	cloud top brightness temperature (bt)
β	ratio of absorption coefficients - "the exponent"
T_s	channel 4 surface bt
δ_s	channel 4 - channel 5 surface bt difference

The fitting algorithm needs a first guess for all four, and then it tries to find the best fit by iterative adjustments. The first two parameters are always left free for the fitting algorithm to solve, but T_s and δ_s could be fixed using forward radiative transfer estimates for their values. If 'nfree' configuration value is set to 4, then no fixing is done. If it is set to 3, then the first three parameters are free, and the curve fitting is tried several times for fixed δ_s values which deviate from the first guess by an increasing amount, but within some reasonable interval. If the 'nfree' parameter is set to 2, then the first two parameters are free, and the curve fitting is similarly tried several times with both T_s and δ_s having fixed values around the first guess point. With the implemented least-squares algorithms the 'nfree' mode 3 gave convergent results most often, hence it is the default.

The configuration settings that set the quality control limits are the following.

```

SETTINGS['max_rmse'] = 0.6 # Distribution max rms deviation
SETTINGS['min_p'] = 0.001 # Distribution min probability

```

'max_rmse' is the largest acceptable root mean square deviation of the brightness temperature difference $T_4 - T_5$ values (i.e. the y_i values) from the best fit curve. 'min_p' on the other hand is the smallest acceptable probability for the distribution χ^2 value to be as large (or larger) than the value from the actual distribution when assuming the best fit model. The quality control scheme rejects the result if both requirements are not met for the segment.

With unlimited processing time the least-squares fitting results from all four segmentation position modes can be examined. However, when the

processing must be completed in a given time, the following parameters may be set to define a less exhaustive search for the solutions.

```
SETTINGS['shift_modes'] = 2    # no of shift mode passes (1-4)
SETTINGS['sub_results'] = 1     # shift mode parameter
SETTINGS['seg_fraction'] = 0.1 # shift mode parameter
SETTINGS['sub_fraction'] = 0.2 # shift mode parameter
```

The value of 'shift_modes' defines the number of segmentation grid positions that will be used for the image. We have already described the details of this option at the beginning of this section. The value of 'sub_results' defines how many fittings are attempted for each subsegment. This could be set to four if all four shift-modes are being used, or even higher as there may be both "over-land" and "over-water" solutions. On the other hand a low value will speed up the processing, as the segment will be skipped in further shift modes if all its subsegments already have the desired number of solutions. Note that this option does not cause exclusion of subsegments from the final results in the case when there are fewer solutions than the value of 'sub_results'. The other two parameters speed up the processing by skipping segments that have few target pixels. The parameters 'seg_fraction' and 'sub_fraction' define the threshold fractions of target pixels within the segment and within any of the subsegments, respectively, which indicate the need to process the segment. With sufficient computing speed these two parameters can be set to zero.

4.3 Graphical user interface

Adding the X argument to the end of the command line when starting `ctth.py` makes the program start interactive graphical window mode, e.g.

```
> ctth.py 200009241343 cliwanet_north noaa14 X
```

In this mode the program will not start to process the data. It expects the pass to have been processed earlier, so that in this case the files

```
200009241343.cliwanet_north.noaa14.ctth.dat
200009241343.cliwanet_north.noaa14.ctth_ott.gif
```

would need to be available in the current directory, containing the processing results and the result gif-image, respectively. The interface shows the resulting image in a window, as shown in figure 3, and offers some pull-down menus for selecting the satellite pass and image to display, for changing the processing options and for defining the mouse functions.

Processing of a given segment can then be requested simply by clicking the image location of interest. The least-squares fitting algorithm output can be checked from the starting window, and if defined in the mouse menus, the

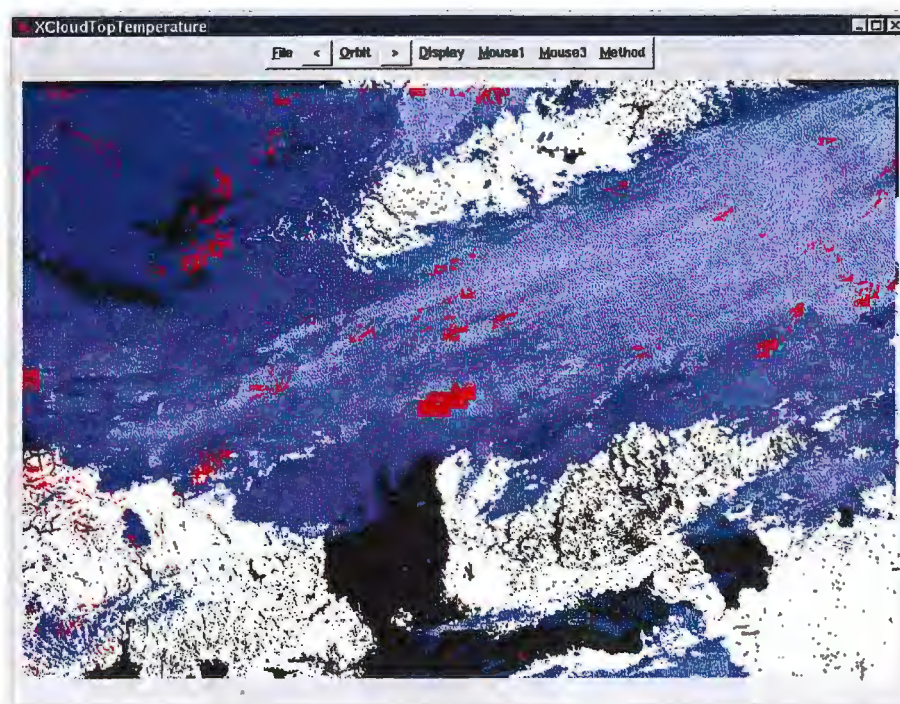


Figure 3: Screen capture of the GUI window.

histograms will be shown in new windows, as shown in the screen capture in figure 4.

The graphical interface provides an overall evaluation tool for the cloud top temperature product. Segments that have no solution, or segments that show distinctively different results from their environment can be identified and processed again. The output from the algorithm together with the histogram windows show the processing details for the segment and allow evaluation of the quality control settings performance. In the later versions of this prototype software more display options for the input data could be added to help in identifying the meteorological situation in the selected segments.

4.4 Radiance ratioing computations

The module `radratio.py` implements the radiance ratio method for obtaining the cloud top temperature estimate from HIRS observations. The module can be started in a similar way as `ctth.py`, i.e. by specifying the satellite pass and a region with the command line parameters. The command to start processing could for example be

```
> radratio.py 200009241343 cliwanet_north noaa14
```

The module reads the output produced by `ctth.py` together with the file con-

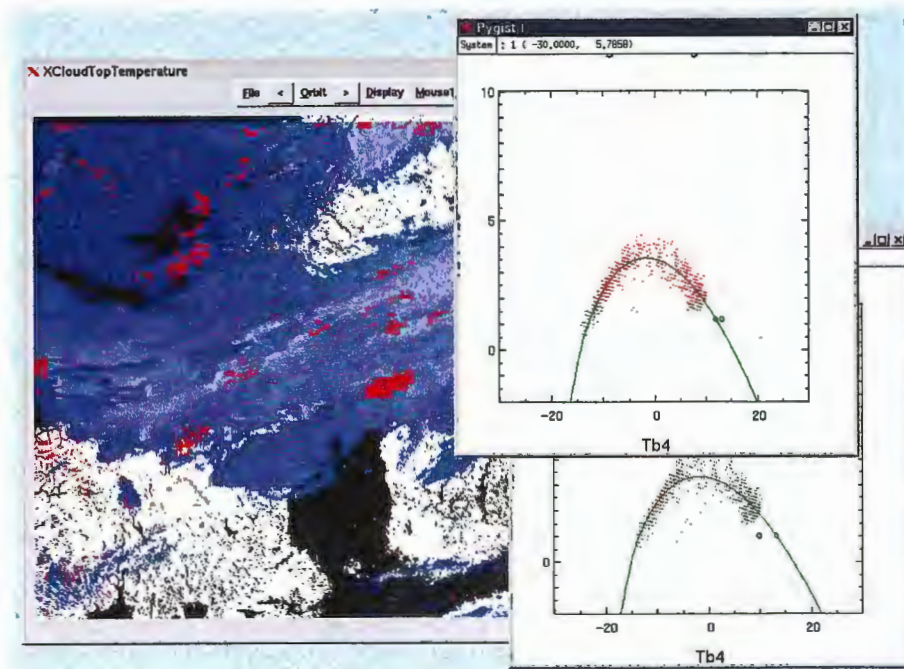


Figure 4: GUI display of the model fit for a requested segment.

taining AAPP processing results for HIRS data. After computing the radiance ratio estimate for each HIRS fov it then compares these results against the nearest histogram method results. The program reports the bias and standard deviation for the two methods.

5 $(T_4 - T_5)/T_4$ histograms - General performance

Successful model fits must be subjected to quality control checks, in order to eliminate various misfits. In some segments the pixel distribution can be limited to a narrow channel 4 brightness temperature range, so that only a short part of the full arc is present. Model fits however may be successful, and in some cases can produce highly erroneous results for the CTT (see figure 18). This can be eliminated through the parameter limits which are set at the python module and passed to the Fortran subroutine controlling the least-squares fitting. Only results where all four parameters have values within the limits will be accepted. In the current implementation we used the ranges T_c in $[-50, \min(T_4)]$, β in $[1, 2]$, δ_s in $[0, \min(T_4 - T_5)_{clear}]$ and T_s in $[\max(T_4), fg+5]$, where fg is the forward model first guess for the cloud clear brightness temperature.

Another obvious problem arises from any image segment where multiple cloud layers are present. Figure 5 shows an example case with two cloud layers. The first-guess surface brightness temperature is shown with the black circle near 10° C. There seems to be one cloud layer with opaque

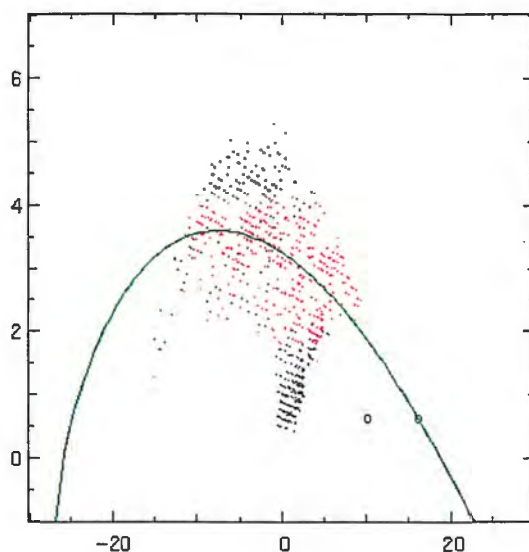


Figure 5: *Model fit in the presence of a dual layer cloud field.*

cloud pixels at temperature near zero, and another cloud layer at temperature near -18° C. Semi-transparent cloud at the lower level, when not obscured by the upper level forms the arc in the bottom right part of the distribution, where T_4 varies between 0° and 10° C. Semi-transparent cloud at the higher level, when there is no lower layer forms the top arc, where T_4 varies between -18° and 10° C. The third arc at the bottom left part of the distribution is formed by semi-transparent cloud at the higher level, when the

background is opaque cloud at the lower level. Finally the inside region of the distribution is formed when the two cloud layers both are transparent in various degree.

The model fit tries to compromise between the three arcs, and inevitably fails to retrieve either of the two cloud temperatures correctly. The resulting cloud top temperature is too cold and is rejected by applying quality control checks. In this case the rmse of the distribution is 0.704 K against the assumed model, so that a limit 0.7 for the rmse would correctly reject the result, but a safer limit below 0.7 is suggested by this example. With a more sophisticated histogram analysis the two cloud layer temperatures could be retrieved, but even then it would be difficult to assign the temperature and height to the semi-transparent pixels because the three distributions overlap.

In the case when there is a lower level opaque cloud filling the segment, and a semi-transparent layer above, the histogram method can still retrieve the upper level temperature. The parameters T_s and δ_s have non-relevant (cloud-clear surface) first guess values for the case, but during the least-squares fitting they can still become adjusted to the opaque cloud values.

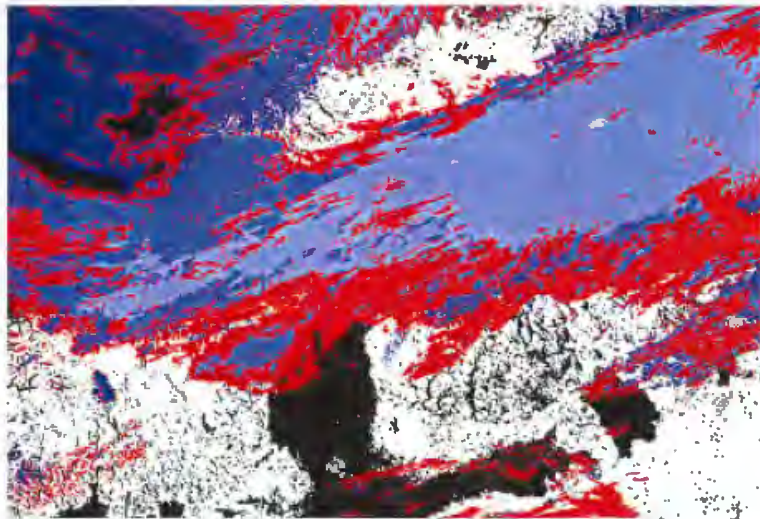


Figure 6: NOAA14 satellite pass at 24-Sep-2000 1434 UTC. Cloud top temperature in opaque cloud pixels, determined from uncorrected AVHRR radiances, are shown in blue colours. The remaining cloudy pixels, which require the correction are shown in red.

To give an example of the overall performance we show here the resulting cloud top temperature images when we apply the histogram method to the case shown in the cover image, or again in figure 6. Of the target pixels shown in red 91% in this particular case were classified as semi-transparent, and 9% as fractional. For the two test runs we set the rmse quality control threshold to 0.7 In the first testrun we used only the fixed image segmenta-

tion ('shift_modes' = 1), and the result image is shown in figure 7. Of all the target pixels in the image 65% got the cloud top temperature retrieved.

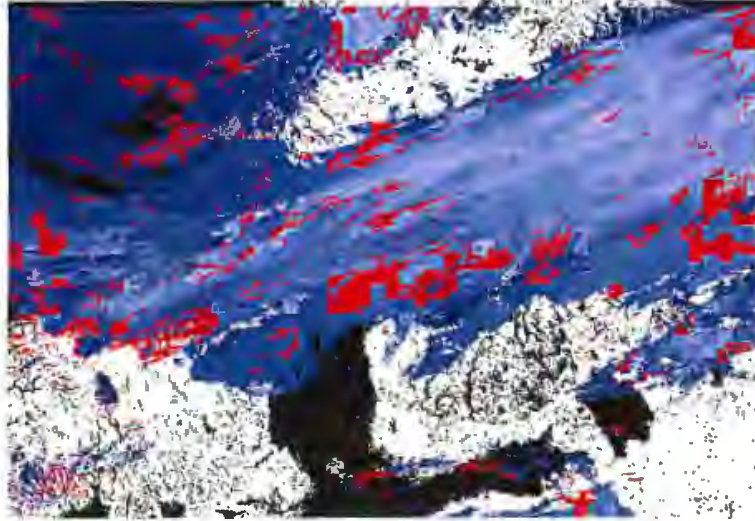


Figure 7: *Histogram method applied with a fixed image segmentation.*

When applying shifted segmenting, the number of segmentation positions as well as the thoroughness of the search can be specified, leading gradually to the best possible result coverage. In the second testrun we used all four segmentation positions ('shift_modes' = 4) together with the most thorough search, and the result image is shown in figure 8. Of all the target pixels in this case 91% got the cloud top temperature retrieved, while the computing time became about three times as long as in the first case.

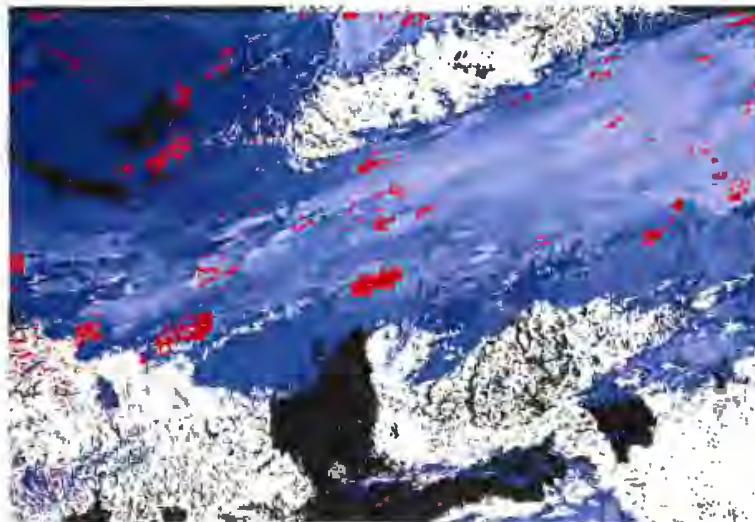


Figure 8: *Histogram method applied with full shifting segmentation.*

6 Validation

Validation of cloud top temperature/height retrievals from satellite data is a well known problem. It is difficult to obtain independent verifying measurements, co-located in time and space, and further these measurements often do not directly provide a "ground truth", but give a rather indirect measure which needs further interpretation, sometimes requiring rather advanced techniques.

To deal with this problem we have chosen to explore several different independent data sources. We are trying to establish a useful validation of the histogram method by comparing against other satellite retrieval techniques and by utilising both ground based observations and flight reports of cloud observations. It will be obvious from the discussion below that more data are needed in order to draw firm conclusions, but hopefully what follows will show a useful procedure for further validation studies.

In section 6.1 we present the different data sources, including the satellite data itself. In the following sections from 6.2 till 6.4 we present the results of the histogram analysis for a few selected cases, and compare the results with the validation data. Section 6.2 compares the results with those of an opaque retrieval. In section 6.3 the results are compared to manual observations from a few of the daily routine flights of the Swedish Airforce. Finally in section 6.4 we compare the retrieval results against ground base remote sensing measurements and radiosonde data.

6.1 Data

The validation study was performed primarily on data from August and September 2000, coincident with the first intensive observation campaign (CNN1) of the EU Framework 5 project CLIWA-NET (see <http://www.knmi.nl/samenw/cliwa-net/>), and secondly on a short period of one week of data in November 2000.

6.1.1 Satellite data

We used locally received (at Norrköping) satellite data from the operational satellites NOAA 12 and 14. The raw hrpt (hfm format) data was ingested into AAPP, and the AVHRR level 1b data calibrated, geo-located, and then remapped (using nearest neighbour resampling) to a Lambert Azimuthal Equal Area projection having a pixel resolution of 1km. The region of interest was The Baltic Sea drainage basin. The region was divided in two sub-regions as specified in table 1.

The HIRS level 1b data were calibrated and geo-located, and kept in satellite projection. Since the level 1b data contains geo-location data for

Projection coord.	central meridian:	60.0N
	central parallel:	20.0E
Scale	horozontal - x:	1000m
	vertical - y:	1000m
Size	horozontal - x:	1670
	horozontal - x:	1134
<i>cliwanet north area</i>		
Area extent (meters)	lower left x,y:	(-726561.014, -87494.003)
	upper right x,y:	(943438.986, 1046505.997)
<i>cliwanet south area</i>		
Area extent (meters)	lower left x,y:	(-726561.014, -1221494.003)
	upper right x,y:	(943438.986, -87494.003)

Table 1: *Projection and area specification for the two areas covering the Baltex Sea drainage Basin*

each HIRS FOV no interpolation or remapping was needed before processing and comparison with AVHRR.

6.1.2 Radiosondes

Radiosonde data are sometimes, and especially in cases of low clouds, able to give at least a rough indication of the height of the cloud base and the cloud top. Six-hourly radiosonde data from the few available stations in the region was stored during the fall of 2000 for this purpose, namely to validate the histogram method in situations with low level clouds.

6.1.3 Ground based measurements

During the CLIWA-NET campaign CNN1, remote sensing techniques from ground based instruments at a few sites in northern Europe were employed. Ceilometers and IR-radiometers provide data for estimating cloud base, and sometimes cloud top, height. The sites in our area of interest encompass Kiruna (21.1E; 67.9N), Onsala (11.9E; 57.4N), Potsdam (13.1E; 52.4N), Lindenberg (14.1E; 52.2N), Helsinki (24.8E; 60.2N), and St. Petersburg (30.7E; 59.9N).

6.1.4 Manual reports from Swedish airforce flight missions

An informal cooperation between SMHI and the Swedish airforce base in Linköping was setup in the late autumn of 2000, with the purpose of getting "cloud truth" information for the validation and improvement of satellite based cloud retrievals developed at SMHI.

Weather flight missions from the Airforce base in Linköping (and from other places in the country) are fairly regular, and are done typically once per day, and usually in the late morning. During these weather surveys, the accompanying meteorologist observes cloud conditions and reports back to the Meteorological office on the ground. Most of the time the aircraft flies in and above the clouds, and when above the cloud top, the height, and sometimes the cloud top structure, is observed.

The collection and transfer of data from the airforce base to SMHI on the one side, and the collection and co-location of satellite data on the other side, required significant manual interaction and effort, and would not be straightforward to automate. Also the quality of these data for validation of the CTT/H algorithm is still uncertain. For instance, the exact earth-coordinates are not easily extracted in the process described above, but instead the cloud observations are geo-located by referring to cities, lakes, or similar ground control points, which may not always be sufficiently exact, and which in some cases can be ambiguous.

Therefore, in order to assess the feasibility of the setup, in terms of cost-benefit, a one week pilot study was performed in late November. This one week, giving only 4 observations, proved to be too short, especially considering the poor satellite coverage in the late morning at that time (only NOAA 12 and NOAA 14 available). Also, the frequently rather complex cloud field observed made the data analysis particularly difficult. It was therefore decided that this pilot study should be extended to include a few more weeks of intercomparison, before a fair conclusion on the feasibility can be made. A further collection effort continued in April and September 2001, giving 10 more cloud top observations, which have yet to be analysed.

6.2 Comparison against opaque retrieval

Maybe the most basic validation of the window technique and the retrieval of the cloud top temperature and height of semi-transparent clouds, is to make a comparison with the results of the opaque retrieval. Most often the cloud field is a mixture of semi-transparent and more opaque clouds. Using the opaque retrieval there will thus often be a cloud top temperature or height available in the neighbourhood to compare with. Of course, the quality of the cloud top temperature and height derived using the opaque retrieval will depend on the complexity of the cloud field (sub pixel cloudiness is not treated properly) and the quality of the cloud mask and type. It is the Cloud Type algorithm which determines if the cloud is opaque or semi-transparent, and what is determined as opaque will not always be truly opaque. Therefore, such a validation against the opaque retrieval needs to be done carefully and will have to be carried out on a case study basis.

We have selected 20 cases from September 2000, during the CLIWA-

NET campaign CNN-1. The selection has been done so as to cover different weather situations, but favouring situations with thin cirrus. We have derived the cloud top temperature using both the straight forward, and operational, opaque retrieval, and the histogram method. Below we include results from two of these cases.

6.2.1 14:46 UTC, September 2, 2000

We focus on the *cliwanet north* area where a frontal band of high clouds cover north eastern and central Sweden. Particularly in the middle of the area where the frontal cloud band seems to dissolve (or where the two bands are merging) over the eastern parts of Sweden and over the Baltic sea a lot of thin cirrus are observed. Most of the time the cirrus clouds seem to be overlying middle or lower clouds. We know that these (multi layer) conditions are not the best for the semi-transparency retrieval, but on the other hand this is an example which is rather representative of the often complex cloud systems observed in reality. In order to justify the use of the histogram technique it must show some skill even in these otherwise complex situations.

In figure 9 we display the cloud top height image of the semi-transparent retrieval only and after merging with the opaque result, together with the channel 3,4,5 RGB and Cloud Type images. It is of course difficult to judge the retrieval in detail from the rather small images shown and the rather coarse height scale. But in general the results seem consistent with the opaque results. We see that the cloud top height is retrieved even for large parts of the lower clouds in the northwest.

If we look a little closer, as in figure 10, we may get a better idea of the performance, though. In figure 10 the semi-transparent results are shown for a small area in the central part of the *cliwanet north* area, together with the merged results of the opaque and the semi-transparent retrievals, and the channel 3,4,5 RGB.

At a first glance it looks as if the retrievals are not in agreement with each other. But the lower cloud height of the opaque retrieval for the cloud band in the central to lower part of the sub-area, as compared to the semi-transparent results, is rather a result of an actual hole in the thin cirrus cloud cover, than an inconsistency. The thin cirrus clouds are overlying a broader middle level cloud deck. The cirrus clouds lie on a height of around 6400 to 7400 meters according to the semi-transparent retrieval.

As an example of the performance of the semi-transparency retrieval we look closer at the four segments corresponding to the 2nd and 3rd column and the 3rd and 4th row (in segment resolution counted from upper left corner) of the close-up shown in figure 10.

In figure 11 we show the two-dimensional histograms and the fitted

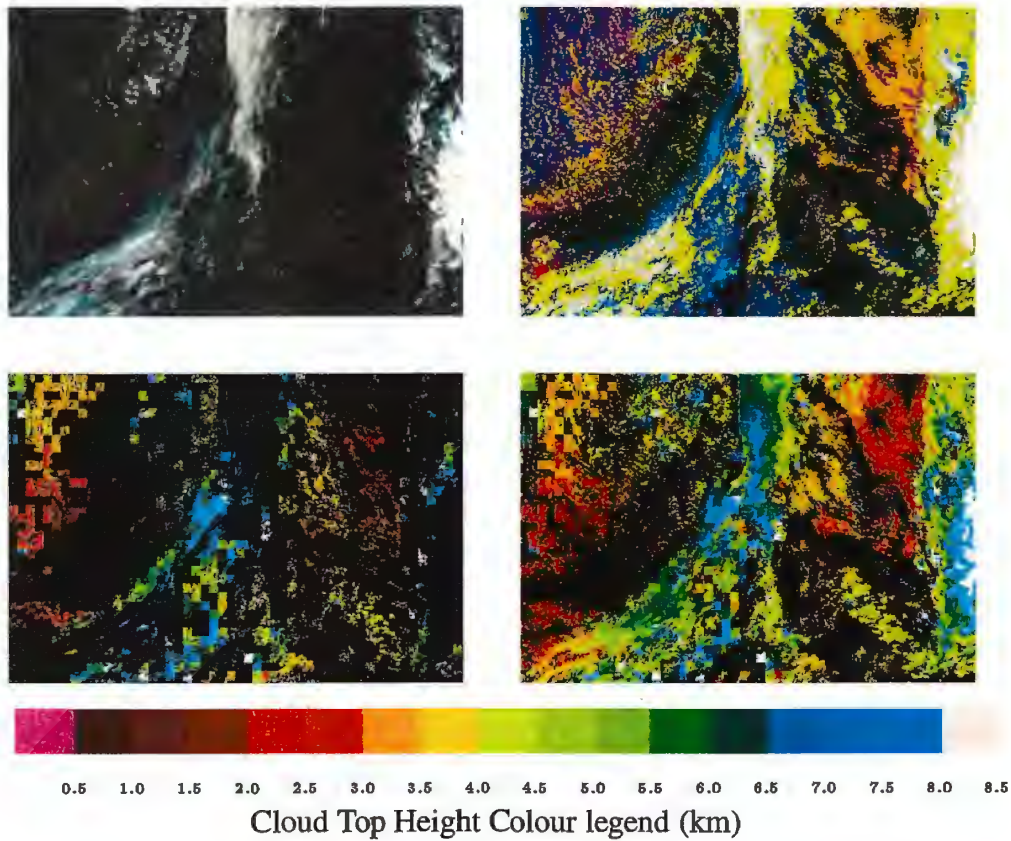


Figure 9: NOAA 12 scene 14:46 UTC September 2, 2000: Channel 3,4,5 RGB (upper left panel), Cloud Type (upper right), and the cloud top height as derived from the window technique only (lower left) and the merged result (lower right) using the opaque results where the window technique fails and where there are no semi-transparent clouds

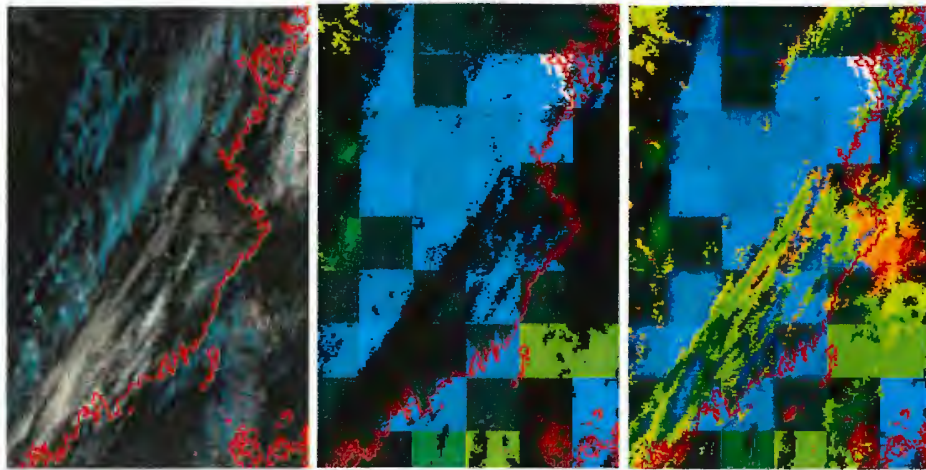


Figure 10: Close-up on cirrus clouds over northern Sweden of the scene shown in figure 9: Channel 3,4,5 RGB (left panel); the cloud top height as derived from the window technique only (middle); and the merged cloud top height for semi-transparent and opaque clouds (right)

curves providing the cloud top temperature results. It is worth being aware here that in the final result we degrade the results to $1K$ and $200m$ resolution, to reflect what is believed to be the best possible accuracy. For the upper left segment the resulting cloud top temperature became $243K$, and the height (above ground) derived using the atmospheric profile of Hirlam was 6400 to 6600 meters. The histogram technique gave 243.70 for the land regime, and 241.63 for the water regime. As the number of water pixels is very small in this segment, the final result is due mainly to the land regime.

In the segment just below the previous one, again two solutions are given, one for the land and one for the water pixels, and as before the land pixels dominate. The result of the land pixels seem realistic, whereas the water pixels are probably too few to provide a reasonable estimate. However, it is hard to judge which is the most correct as there are rather few points on the left leg of the arc (towards the opaque clouds). The results are $240.7K$ and $233.4K$ for the land and sea regimes respectively. The final output of the algorithm is $240K$ and $7000m$ to $7200m$.

The upper right segment of the four displayed in figure 11 does not provide a solution for the few water pixels, but the land regime seem to provide a reasonable estimate of $243.2K$, resulting in a cloud top temperature and height product of $243K$ and $6600m$ to $6800m$. In the upper right corner of this segment there are a few pixels which apparently have been classified as opaque clouds, and where the difference $T_{b4} - T_{b5}$ is too small to be considered for the window technique. According to the opaque retrieval the cloud tops are around $264K$ and $3600m$, and thus significantly lower than

the surrounding semi-transparent cloud tops derived using the window technique. Since the cloud field seems to be multi-layered both estimates could actually be correct at the same time.

In the last, lower right, of the four segments, there are more points on the left leg of the curves (see lower left panel of figure 11) and both the water and the land regimes provide nearly identical estimates. This is of course a good indicator of a reliable estimate, and such information will be passed to the quality flagging process in the possible future product. The cloud top temperature and height becomes $242K$ and $6800m$.

6.2.2 13:28 UTC, September 23, 2000

We focus on the *cliwanet north* area where, much like the case of the 2nd September discussed above (section 6.2.1) a frontal band of high clouds goes from the north and centre in an arc towards the southwestern corner of the area. But in this case the cloud band is more dominated by thin cirrus, and the cloud field is less complex, with larger parts of the area covered with what looks like only one cloud layer.

The cloud top height images (for semi-transparent clouds only and for both opaque and semi-transparent clouds) and the channel 3,4,5 RGB are shown in figure 12. Again it is difficult to judge the retrieval in detail from the rather small images shown, but figure 12 provide an overview of the performance. We observe that there are many white areas indicating that the clouds have rather high tops ($9000m$ or higher), but one may also observe that many cloudy areas are not solved. These frequently unavailable cloud top height estimates are due to the generally rather thin cloud cover (too few pixels in the left part of the two-dimensional histograms).

If we zoom in on the thin cirrus over the Botnian Bay shown in figure 13 we see that the cloud top height is available only for less than half of the cloudy pixels. The cloud top height is around $7000m$ to $8000m$, except for the clouds in the lower left corner of the sub-area, where cloud tops of nearly $10000m$ are found.

The upper left segment of the sub-area apparently have too few land pixels in order to provide an estimate for the land regime (see figure 14). But the water regime nicely produces a cloud top temperature of $246.2K$, giving a cloud top temperature and height output for the clouds inside the segment of $246K$ and $7200m$. We see that the thicker cirrus clouds, which have been detected as opaque, in the northwest have approximately the same cloud top heights of between $6600m$ and $7600m$, which is encouraging for the window technique.

The cloud top temperature retrieval for the segment to the right (next to the one discussed above) seem more problematic when looking at the histogram in the right panel of figure 14. The land pixels are very few, and

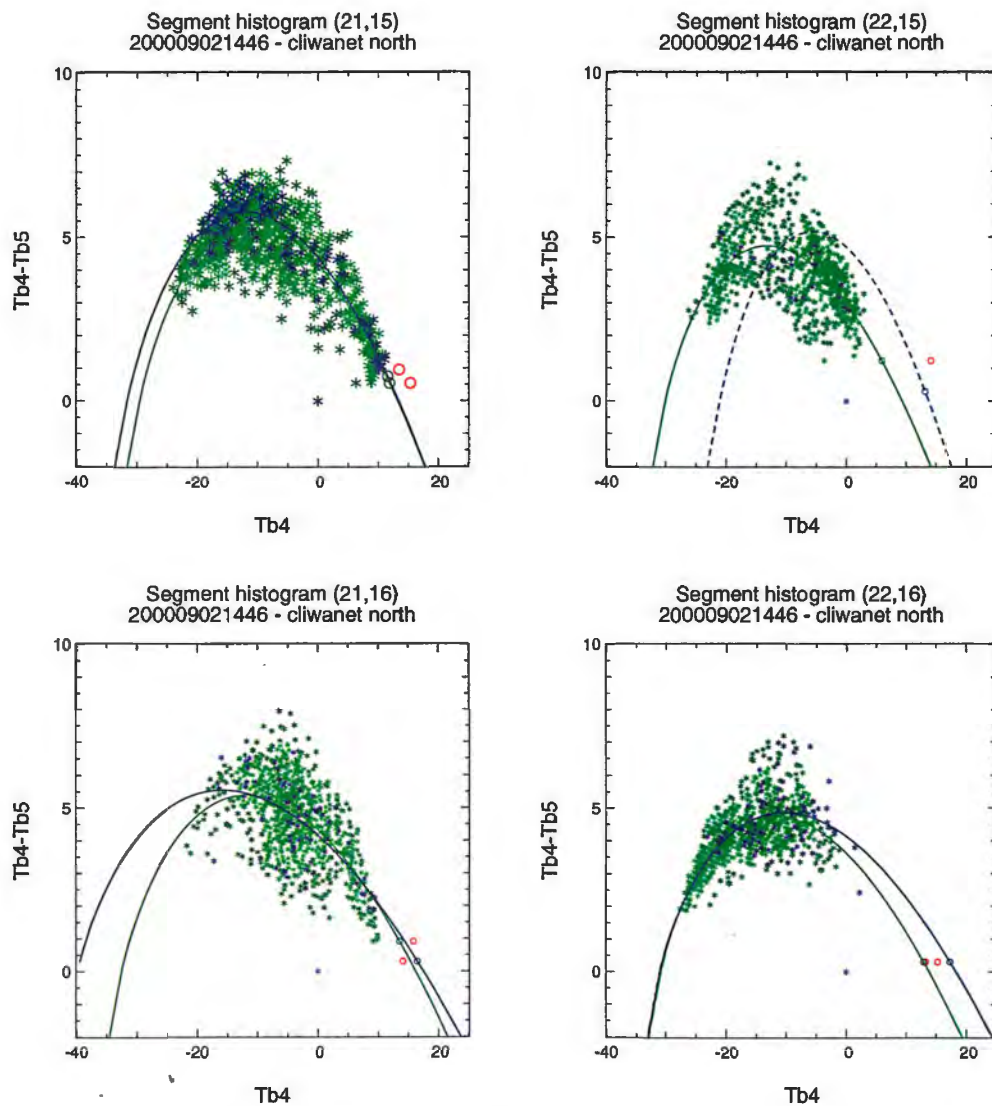


Figure 11: Histogram and fitted curves for the four segments corresponding to the 2nd and 3rd column and the 3rd and 4th row (in segment resolution counted from upper left corner) of the close-up shown in figure 10. The segment numbers of the original cliwanet north area of the NOAA 12 scene 14:46 UTC September 2nd, 2000, are written above the plots. All pixels used in fitting the curves for the land and sea/water regimes are marked with a green (land) or blue (sea) \star . The two red \circ correspond to the cloud free observations for the land and sea regimes. The blue line and \circ are the result of the curve fitting for the sea regime, and the green ones are for the land. The dashed blue curve in the upper right panel correspond to the first guess for the water regime, for which no solution was found.

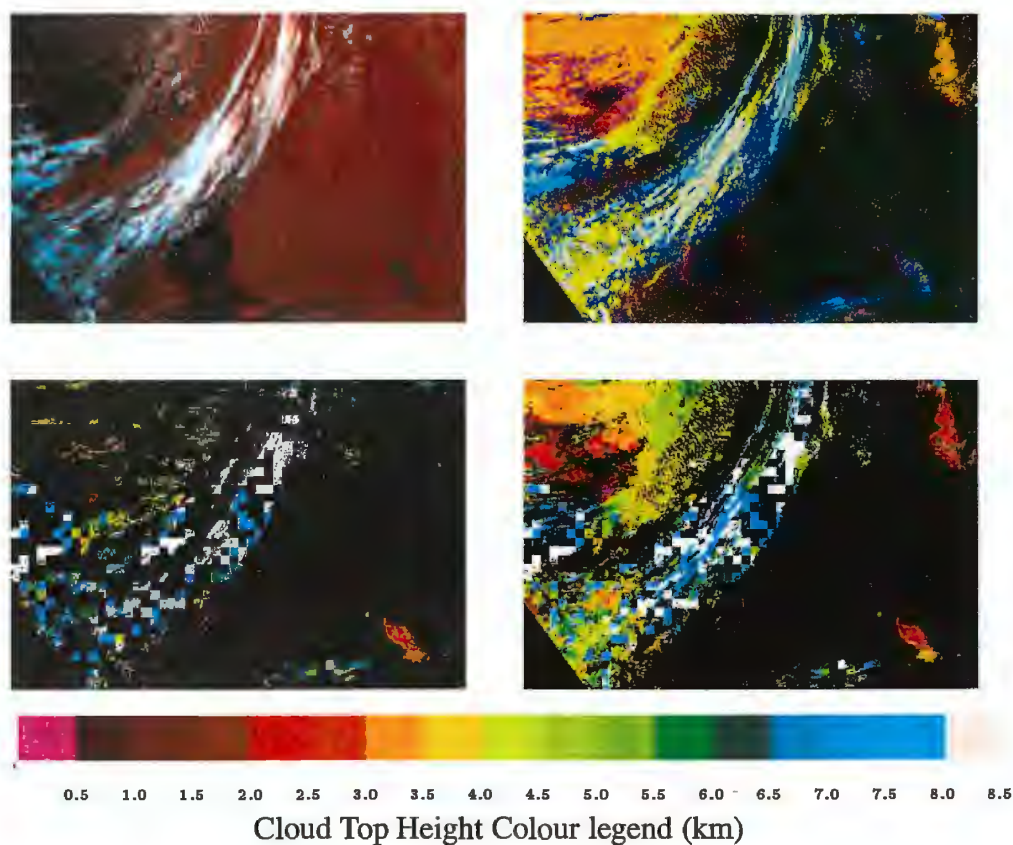


Figure 12: NOAA 12 scene 13:28 UTC September 23, 2000: Channel 3,4,5 RGB (upper left panel), Cloud Type (upper right), and the cloud top height as derived from the window technique only (lower left) and the merged result (lower right) using the opaque results where the window technique fails and where there are no semi-transparent clouds

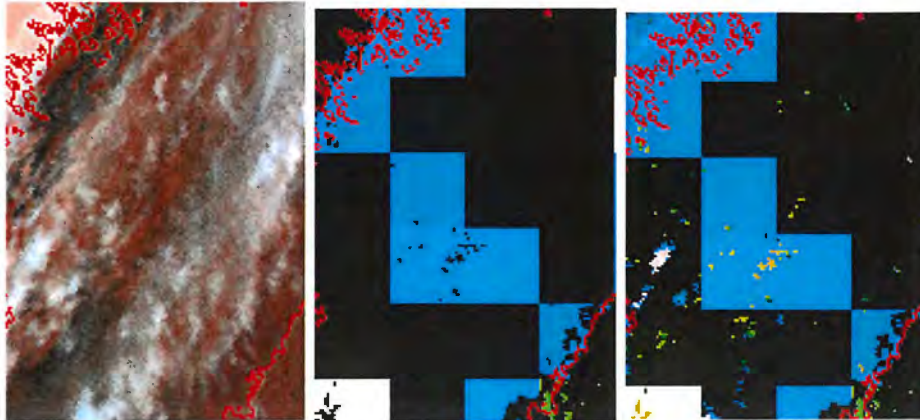


Figure 13: *Close-up on cirrus clouds over northern Sweden of the scene shown in figure 12: Channel 3,4,5 RGB (left panel); the cloud top height as derived from the window technique only (middle); and the merged cloud top height for semi-transparent and opaque clouds (right)*

the cloudy observations over water show a substantial homogeneity with few observations on both the right (towards the clear) and the left (towards the opaque) side of the histogram. The results are $255.7K$ for the land pixels and 246.8 for the sea. Since a major part of the area is over sea the final cloud top temperature and height are $247K$ and $7000m$. Despite the suspicious curve fit the result is in good agreement with the neighbouring segment and thus in this case probably close to reality.

The segment in the second row and the first column of the sub-area shown in figure 13 does not provide a solution for the many pixels over water, but instead for the few pixels over land. Actually this solution seems to fit well with the water regime as well. The result is $245K$ and $7400m$, close to the estimates of the neighbouring segments.

The segment in the 2nd row and 2nd column does not provide a cloud top temperature and height estimate as seen from figure 13, and the histogram plot in the lower right panel of figure 14. The cloud regime is too homogeneous, and there are too few observations on the right and left legs of the arc to provide a good fit.

6.3 Comparison against flight observations

During the initial phase of the pilot study of collection of cloud top observations from weather survey flights performed by the Swedish airforce aimed at validating the cloud top temperature and height algorithms, four observations in early November 2000 were made, as mentioned in section 6.1.4. Here we do not intend to use these 4 cases as a true validation of the semi-transparency retrieval, but merely to illustrate the prospects for validation these kind of data may provide.

As already indicated in section 6.1.4 the cloud field in southern Sweden, where the weather surveys are performed, were often rather complex. Often the cloud field was highly spatially varying and with more than one cloud layer present. In addition three of the flight observations were made more than 2 hours from the closest satellite pass. This, together with the inaccurate position of observation made the data impossible to use in a quantitative validation.

Here we discuss the only case with nearly coincident aircraft and satellite cloud top observations on November 9, 2000. The observations are delivered to SMHI in textform (in Swedish) via email, and for this case it looked like this:

Molnöversida 001109 1440z.
Ref till NOAA-bild 1313z.
Molntopp Linköping - Sommen (sjö 50 km SW Linköping):
2900 m.
S-SW Sommen : molntopp 5000-5500 m.
Uppmätt kl 1440z.

The above can be translated and summarised as:

Cloud top observations at 14:40 UTC, with reference to NOAA AVHRR image at 13:13 UTC: At the lake Sommen (a rather large lake extending from north west around $15.0^{\circ}E$; $58.2^{\circ}N$ to south east around $15.4^{\circ}E$; $57.9^{\circ}N$) a cloud top height of 2900m, and S-SW of the lake Sommen cloud tops around 5000–5500m.

The cloud top observations refer to an area near the edge of a higher cloud overlying a lower cloud deck, in the satellite image at 13:08 UTC (the same as the 13:13 UTC referred to above). We assume that the two observations refer to these two major cloud decks. The approximate area is encircled in the left RGB image shown in figure 15 and in the close-up shown in figure 16.

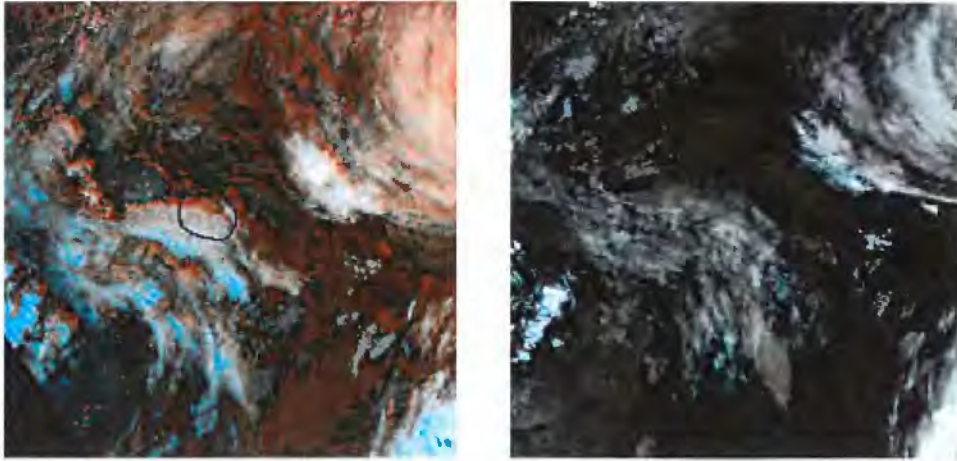


Figure 15: Channel 3,4,5 RGB images of the two consecutive NOAA 14 passes at 13:08 UTC (left) and 14:47 UTC (right) November 9, 2000. The approximate area of interest in southern Sweden is encircled in the image to the left.

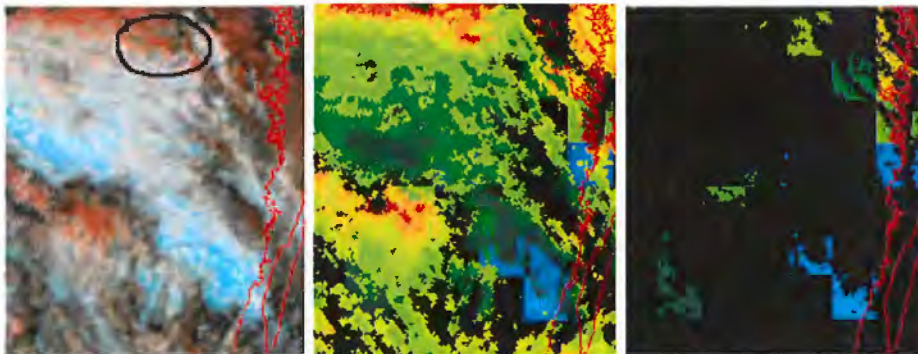


Figure 16: Channel 3,4,5 RGB image (left panel) and cloud top height using both the opaque and semi-transparent retrievals (middle) and the semi-transparent only (right) of a NOAA 14 pass on November 9, 2000, 13:08 UTC. Close-up on the area around and south of the lake Sommen in southern Sweden, where two cloud top observations were made.

From the satellite data at 13:08 UTC we get cloud top heights of 2600m to 3400m in and a little to the north of the marked area, and for the higher cloud deck a little to the south west, referred to, we get cloud top heights of 4800m to 5800m (the green colours in the right panel of figure 16).

Later at 14:47 UTC we get cloud top heights between 2200m and 3200m for the lower cloud deck and approximately 4200m to 5200m for the higher one. The high clouds look more fuzzy and less opaque in the RGB images at this time, indicating that the clouds may be in the process of dissolving. To the north of the area there are several clearly detectable patches of low level clouds which from the cloud top temperature image look rather homogeneous. These clouds have tops around 2600m to 3400m, thus a little higher than what was retrieved closer to the observation point.

Though the above clearly demonstrate the limitations in this kind of intercomparison we can conclude that the satellite retrieval does not contradict the aircraft observations. But as observed in the figures 16 and 17 most clouds are detected as opaque, and therefore a direct validation of the semi-transparent retrieval is not possible. The semi-transparent retrieval proved to be able to add only little extra information here.

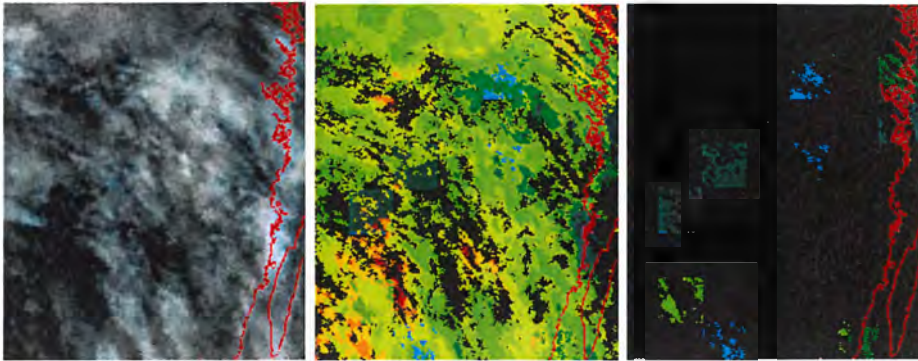


Figure 17: Channel 3,4,5 RGB image (left panel) and cloud top height using both the opaque and semi-transparent retrievals (middle) and the semi-transparent only (right) of a NOAA 14 pass on November 9, 2000, 14:47 UTC. Close-up on the area around and south of the lake Sommen in southern Sweden, where the two cloud top observations were made.

Having verified that the cloud top height of the opaque retrieval fits the observations rather well, one could check nearby areas with results from both the opaque and the semi-transparent retrievals, in order to make an indirect validation of the latter. The two closest segments with some results of the semi-transparent retrieval are found on the border of the higher cloud and the lower cloud just to the east of where we have the cloud top observation of the low cloud, and two segments further to the south (the two segments with cyan colours in the upper part of the image shown in the right panel of figure 17).

The histograms of these two segments are shown in figure 18. In both cases the curve fit is rather good on the land pixels, but the low number of points in the histogram illustrate well the shortcomings of the method in this case. From the points alone it is impossible to see a curved pattern in the histogram. At the northern most segment, on the edge of the higher cloud, the result agrees very well with the opaque retrieval, giving a height of $4200m$ and a temperature of $254K$. The segment to the south give cloud top heights of around $7400m$, or approximately $2000m$ above what is found with the opaque retrieval.

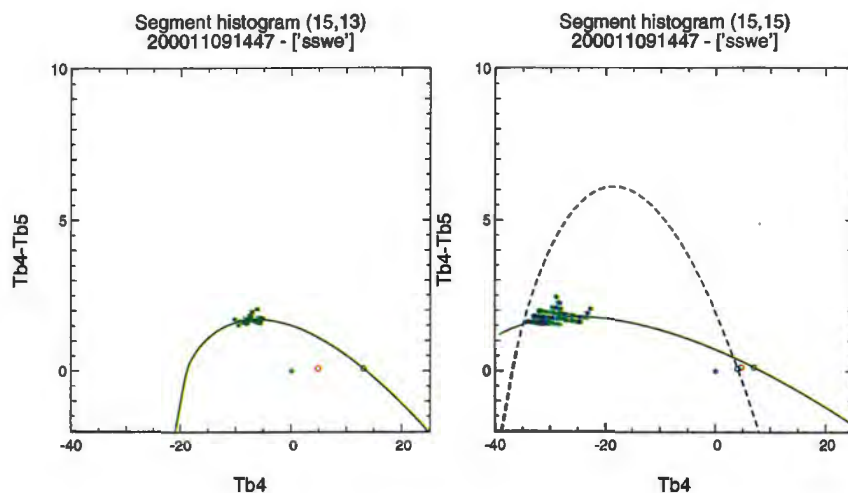


Figure 18: Histograms and fitted curves for two of the few segments in the case shown in figure 17 where the semi-transparent retrieval has provided an estimate. The left panel correspond to the segment with cyan colouring in the second row from above in the right panel of figure 17. The right panel correspond to the segment (also coloured cyan) two rows below.

6.4 Comparison against ground based measurements and radiosondes

Validation against radiosondes can be done qualitatively by viewing the available radiosonde profiles, as shown in figure 19. Using the graphical interface, the profiles can be displayed and the derived cloud top temperature can be used to show the respective pressure level obtained from the temperature profile. This result can be compared against the behaviour of the dew-point temperature profile near the suggested height.

Validation of the cloud top temperature and height retrieval for low clouds using radiosonde data has not been done yet, due to limited resources. Also the validation against data from the ground based observation systems of the CLIWA-NET project is yet to be performed.

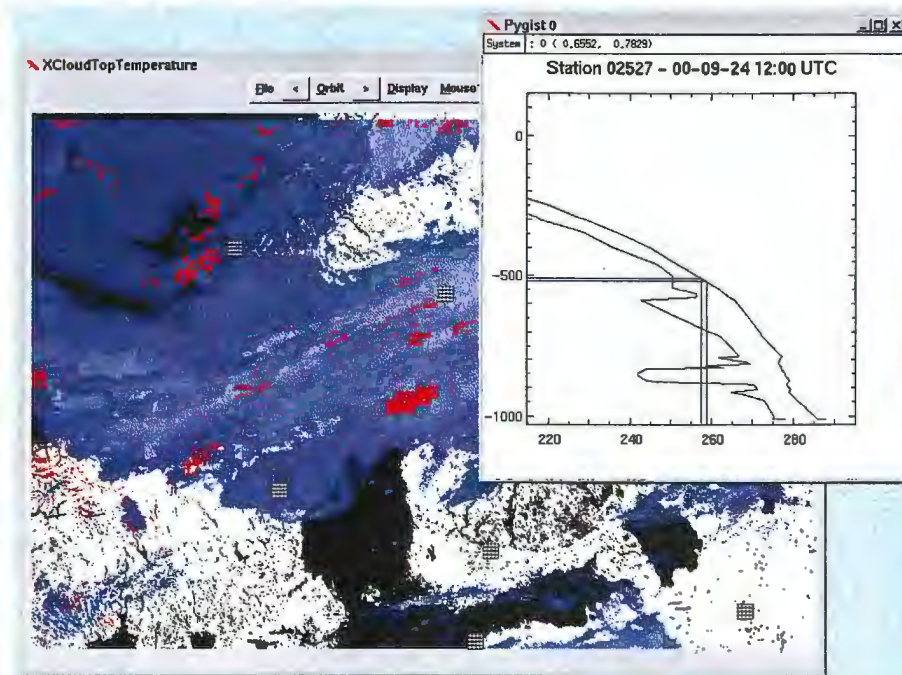


Figure 19: Display of the closest radiosonde profiles to a requested segment, showing the segment minimum channel 4 bt (black lines) and the derived cloud top temperature (blue lines), together with their respective pressures levels.

7 Conclusion and recommendations

Based on the work of Inoue (1985) and Derrien et al. (1988), we have developed software which implements a two-dimensional histogram method for obtaining the semi-transparency correction for the AVHRR near infrared window channel brightness temperatures. This correction is required if the cloud top temperature and height is to be derived over semi-transparent and broken cloud fields.

The experience from this study generally shows that the method works well for pixel histograms with sufficient coverage over the channel 4 temperature range, in which case the histograms can show good agreement between the observed distribution and the theoretical model. But the method is vulnerable to misfits, most often when there is little variance in the cloud transmittance or when there are multiple cloud layers present. Therefore attention must be paid to setting up appropriate quality control tests, with their respective rejection limits.

However, it must be taken into consideration that the implemented method was not tested in winter situations with a cold underlying surface. Such conditions will inevitably limit the channel 4 temperature range, and consequently make the retrieval less successful. In order to better assess the global (meaning central and northern european conditions) performance of the algorithm more Scandinavian winter cases are necessary.

As the required quality control limits tend to reject more segments, we included in the current implementation some methods which help to increase the final coverage of the successful CTT/H assignments. The first method is to increase the CTT/H resolution to subsegment level, which is achieved through shifting the segmentation grid. A further method is to interpolate over this higher resolution subsegment grid. The segmentation shifting processing can be controlled by user specified configuration parameters, and with increasing computing power or less critical processing time requirements, a more exhaustive search for solutions can be chosen.

In addition to the histogram correction software as such, we have developed an interactive graphical user interface for applying the method. This allows particular segments or segment subsets to be selected and displayed, and to start the processing for individual segments and then examine the results and evaluate performance of the quality control settings.

We knew that validation of cloud top temperature and height retrievals in general is a difficult task, and our efforts described herein illustrate some of the problems expected. We did not manage to carry out all of the desired validation tasks, but instead indicated how one may proceed if further resources are provided.

We also prepared software for producing cloud top temperature results from the radiance ratioing method and for comparing them against the re-

sults from the histogram method. Comparison and validation of these data will extend the validations in the future work.

Intercomparison of the results from the opaque and the semi-transparent cloud retrieval methods show in general good agreement in the few cases studied in detail. When both estimates are available the cloud top height derived using the semi-transparent retrieval is always equal or higher than the top height derived using the opaque cloud retrieval. This fact is taken as a sign of health of the histogram method implemented. The sometimes significantly larger cloud top heights of the semi-transparent retrieval do not necessarily imply that these estimates are wrong, but may be due to erroneous cloud top heights derived from the opaque retrieval method.

Clouds are classified as opaque provided the brightness temperature of AVHRR channel 4 is equal to or only slightly higher than at channel 5. This method is based on the assumption that the transparency, of especially ice-particle clouds, increases with increasing wavelength in this part of the spectrum, and that the temperature decreases with height. If this assumption is violated, as e.g. in situations with temperature inversions, clouds classified as opaque may in reality be semi-transparent. In these cases the height derived from the opaque retrieval can be too low.

We carried out a preliminary analysis of aircraft derived cloud top observations to validate the algorithm. Unfortunately the data from the four flights in November 2000 proved to be very difficult to use due to both the time deviations between observations (flight reports and satellite data) and the prevailing rather complex cloud field, which was composed of several cloud layers and had great spatial variability. This kind of validation is very time consuming, but due to the lack of other methods it may prove valuable once a little more data have been analysed.

The algorithm can certainly be refined with further development work. More sophisticated histogram analysis could be applied in the quality control procedure, and the final output needs the resulting quality flags to be defined. Overall, the performance of the histogram method in the implementation described here seems encouraging.

A Software

A.1 ctth_config.py

This is a configuration file which is read by the other Python modules. Editing the global variable values in this file defines the directory names for the input data and sets processing options. Listed below is an example configuration file.

```
# global variable definitions

global PHYSIO_DIR, PREPRO_DIR, AVHRR_DIR, CLOUD_DIR
global AAPP_DIR, RAOB_DIR, SOURCE_DIR
global MF, FIRSTGUESS
global LMASK, PHYSIO, PREPRO, AVHRR, CLOUD, INFO
global SETTINGS
global SEGH, SEGW, SEGNX, SEGNY, RAOBIDX, DISPLAY
global FILE, TIME, AREA, SAT, REG, RES
global TRUE, FALSE, FNOVAL
TRUE = 1
FALSE = 0
FNOVAL = 999999.

# directory names

PREFIX = "/home/data/CTTH"
PHYSIO_DIR = PREFIX + "/phys"
PREPRO_DIR = PREFIX + "/prepro"
AVHRR_DIR = PREFIX + "/avhrr"
CLOUD_DIR = PREFIX + "/cloud"
AAPP_DIR = PREFIX + "/aapp"
RAOB_DIR = PREFIX + "/raob"
SOURCE_DIR = PREFIX + "/src"

# Default settings
# Some of these may be changed by command line options
```

```

SETTINGS = {}
SETTINGS['runmode'] = "batch" # batch / xwindow
SETTINGS['verbose'] = 0 # Output print level 0,...,7,..
SETTINGS['lsqname'] = "starpac" # Lsq routine
SETTINGS['nfree'] = 3 # No of free parameters
SETTINGS['segw'] = 32 # Segment width
SETTINGS['segh'] = 32 # Segment height
SETTINGS['max_rmse'] = 0.6 # Distribution max rmse
SETTINGS['min_p'] = 0.0 # Distribution min probability
SETTINGS['shift_modes'] = 1 # shift mode passes (1-4)
SETTINGS['sub_results'] = 1 # shift mode parameter
SETTINGS['seg_fraction'] = 0.25 # shift mode parameter
SETTINGS['sub_fraction'] = 0.50 # shift mode parameter

```

A.2 ctth.py

This module is the main program, which reads the configuration file and starts the processing of the data for a given satellite pass over a given region. The processing request is specified through command line arguments in the form

```
> ctth.py <yyyymmddhhmi> <area> <satellite>
```

or alternatively, the arguments can be given with a single string containing the arguments separated by dots, in the form

```
> ctth.py <yyyymmddhhmi.area.satellite>
```

The processing start command could, for example, be

```
> ctth.py 200009241343 cliwanet_north noaa14
```

Data specification from the arguments together with the directory names from the configuration file are used to locate the input data files required for the processing. After reading the input data ctth.py starts the processing by calling the method cloudtop.temperature. The processing method is discussed in depth in section 4.2.

Once the processing has completed for a certain pass, and the output files have been produced, ctth.py can be started in an interactive graphical window mode, as described in section 4.3. The command in this case would be

```
> ctth.py 200009241343 cliwanet_north noaa14 X
```

A.3 cloudtop.py

Module cloudtop.py implements the method cloudtop.temperature, which is the main processing subroutine for the data provided by ctth.py. By calling

appropriate subroutines in this module `cloudtop.temperature` handles both the full processing mode and the graphical interface mode.

A.4 `cttsegment.py`

Module `cttsegment.py` is called by the `cloudtop` module in interactive mode. When the user selects a segment to be processed again, the details of the processing are written into a temporary file. This filename together with the segment dimensions are passed to `cttsegment.py` as arguments. `Cttsegment.py` then plots the histogram and the model fit in a new window that appears on the screen.

A.5 `radratio.py`

The module `radratio.py` implements the radiance ratio method for obtaining the cloud top temperature estimate from HIRS observations, as described in section (3.3). The module can be started in a similar way as `ctth.py`, i.e. by specifying the satellite pass and a region with the command line parameters. The processing command could, for example, be

```
> radratio.py 200009241343 cliwanet_north noaa14
```

The module reads the output produced by `ctth.py` together with the file containing AAPP processing results for HIRS data. After computing the radiance ratio estimate for each HIRS fov it then compares these results against the nearest histogram method results. The program reports the bias and standard deviation for the two methods.

A.6 C extensions in `ctth_cmod.C`

Compiled extensions to Python are most commonly implemented with C routines, so that standard methods for the calling interface Python/C can be easily applied. Therefore, although the extension subroutines needed by `cloudtop.py` come from software packages coded in Fortran, a C-interface was introduced as a layer between Python code and the Fortran subroutines. Subroutines or C-modules in an imported object file are seen as methods from Python, and `ctth_cmod.c` implements the following five methods.

`ctth_cmod.cttfite`

This method is the interface to the least-squares fitting computation for data from a given segment. The call is of the form

```
lsqfit = ctth_cmod.cttfite(  
method, firstguess, limits, verbose, segarea, t4, d45, flags)
```

and the subroutine reads the data passed in the arguments, and calls the Fortran subroutines in an appropriate way. *method* is the identifier for the least-squares fitting method, which can be selected in the configuration file. *firstguess* is for passing the four parameters (*fgtc*, *fgbeta*, *fgts*, *fgdt*) that specify a first guess for the model fit to the segment data. *limits* specifies an acceptable range for each of the four parameters. *verbose* is a numeric value which can be set in the configuration file, and which indicates how much log output should be produced during the computations. *segarea* gives the size of the segment, also set up in the configuration file. *t4* contains the channel 4 brightness temperatures for the segment pixels, and *d45* contains the difference of channel 4 and 5 brightness temperatures. *flags* is an array of the same size as *t4* and *d45* and indicates which pixels should be used in the model fitting.

The return value from the subroutine is a set of four parameters together with goodness of fit estimators, (*tc*, *beta*, *ts*, *dt*, *rmse*, *p*). The parameters specify the best fit of the model to the data, and the variable *rmse* gives the RMSE of the distribution from the best model. Negative values mean failure in the fitting. Variable *p* estimates the fit in terms of the probability of the distribution with the given model.

ctth_cmod.start_rtov

This method can be used to invoke RTTOV forward computations for a single segment. In the graphical user interface mode this feature can be selected as one of the mousebutton-1 options. RTTOV output is then part of the information returned when the user points and selects a segment.

ctth_cmod.process_rtov

This method is called from *radratio.py* and it passes the cloud top temperatures obtained by histogram method to the program *radratio.F*. *radratio.F* then compares the results against the cloud top temperatures obtained from radiance ratioing method.

ctth_cmod.segsave

This method is called from *cloudtop.py* in graphical interface mode, when model fitting has completed for the chosen segment. Data for the segment together with the model fit are stored in a temporary file.

ctth_cmod.segload

This method is called from *cttsegment.py* in the interactive mode when reading in data for the segment to be plotted.

A.7 Fortran modules in `ctth_fmod.F`

This module contains the Fortran subroutines that are called by data passing C-routines in the `ctth_cmod` interface. The subroutines rearrange the data into the form required by the software package programs (in Numerical Recipes and Starpac) and control the data processing for finding the best model fit in one segment. The module contains the following subroutines.

cttfif

This is the main subroutine controlling the best fit search. Depending on the chosen method in the configuration file it calls an interface routine either for Numerical Recipes (`fit_mrqlmin`) or Starpac (`fit_nlsd`). In the configuration file one can also define the number of free parameters in the set (`tc,beta,ts,dt`) as they are passed to the least-squares fitting algorithm. Depending on this choice `cttfif` varies the remaining "fixed" parameters around the firstguess, and calls the fitting algorithm repeatedly to find the best fit.

fit_mrqlmin

This subroutine calls the least-squares fitting algorithm in the Numerical Recipes software.

mrql_mdl

`mrql_mdl` implements the model and its derivatives in a subroutine that Numerical Recipes subroutines can call.

fit_nlsd

This subroutine calls the least-squares fitting algorithm in the Starpac software.

nlsd_mdl

`nlsd_mdl` implements the model in a subroutine that Starpac subroutines can call.

nlsd_drv

`nlsd_drv` implements the model derivatives in a subroutine that Starpac subroutines can call.

fittest

After finding the best fit parameters of the model the subroutine `fittest` is called to compute the goodness of fit estimators, RMSE and p , which will be returned to the calling python module. Using this subroutine, instead

of returning the quality control value from the applied algorithm makes the fitting task consistent as seen from python level.

A.8 radratio.F

This subroutine runs RTTOV to produce cloud top temperatures with the radiance ratioing method, and compares the results against the temperatures obtained by the histogram method, and passed in through an argument array.

A.9 Fortran subroutine packages

Numerical Recipes

The *Levenberg-Marquardt method* for nonlinear least-squares fitting is implemented in Numerical Recipes in the subroutine mrqmin. Together with the subroutines which become called by mrqmin the required modules are covsrt.F, gaussj.F, mrqcof.F, mrqmin.F, gammln.F, gammq.F, gcf.F and gser.F.

Starpac

STARPAC (Standards Time Series and Regression Package) freeware is a portable library of Fortran routines for statistical data analysis from the National Institute for Standards and Technology (NIST). Information about the software together with links for downloading the code and a User's Guide can be found at <http://www.scd.ucar.edu/softlib/STARPAC.html>.

References

- Derrien, M., L. Lavanant, & H. L. Gleau, Retrieval of the cloud top temperature of semi-transparent clouds with avhrr, in Proceedings of the IRS'88, Lille, France, pp. 199–202, 1988.
- Inoue, T., On the temperature and effective emissivity determination of semi-transparent cirrus clouds by bi-spectral measurements in the 10 μm window region, J. Met. Soc. Japan, 63, 88–98, 1985.
- Press, W. H., B. P. Flannery, S. A. Teukolsky, & W. T. Vetterling, Numerical Recipes, Cambridge University Press, Cambridge, 1986.
- Putsay, M., M. Derrien, H. L. Gleau, & G. Monnier, Comparison of two methods to estimate the cloud top temperature and pressure for noaa-avhrr and hirs data, in Proc. 1999 Eumetsat Meteorological Satellite Data User's Conference, Copenhagen, Denmark, pp. 199–202, Eumetsat, Darmstadt, 1999.
- Smith, W. L., H. M. Woolf, P. G. Abel, C. M. Hayden, M. Chalfant, & N. Grody, Nimbus-5 sounder data processing system, Tech. rep., NOAA NESS 57, 1974.
- Wu, M.-L. C., A method for remote sensing the emissivity, fractional cloud cover and cloud top temperature of high-level, thin clouds, J. Clim. Appl. Meteorol., 26, 225–233, 1987.

SMHIs publiceringar

SMHI ger ut sex rapportserier. Tre av dessa, R-serierna är avsedda för internationell publik och skrivs därför oftast på engelska. I de övriga serierna används det svenska språket.

Seriernas namn	Publiceras sedan
RMK (Rapport Meteorologi och Klimatologi)	1974
RH (Rapport Hydrologi)	1990
RO (Rapport Oceanografi)	1986
METEOROLOGI	1985
HYDROLOGI	1985
OCEANOGRAFI	1985

I serien METEOROLOGI har tidigare utgivits:

1985

- 1 Hagmarker, A. (1985)
Satellitmeteorologi.
- 2 Fredriksson, U., Persson, Ch., Laurin, S. (1985)
Helsingborgsluft.
- 3 Persson, Ch., Wern, L. (1985)
Spridnings- och depositionsberäkningar för avfallsförbränningsanläggningar i Sofielund och Högdalen.
- 4 Kindell, S. (1985)
Spridningsberäkningar för SUPRAS anläggningar i Köping.
- 5 Andersson, C., Kvick, T. (1985)
Vindmätningar på tre platser på Gotland. Utvärdering nr 1.
- 6 Kindell, S. (1985)
Spridningsberäkningar för Ericsson, Ingelstafabriken.
- 7 Fredriksson, U. (1985)
Spridningsberäkningar för olika plymlyft vid avfallsvärmeverket Sävenäs.
- 8 Fredriksson, U., Persson, Ch. (1985)
NO_x- och NO₂-beräkningar vid Vasaterminalen i Stockholm.
- 9 Wern, L. (1985)
Spridningsberäkningar för ASEA transformers i Ludvika.
- 10 Axelsson, G., Eklind, R. (1985)
Ovädret på Östersjön 23 juli 1985.
- 11 Laurin, S., Bringfelt, B. (1985)
Spridningsmodell för kväveoxider i gatumiljö.
- 12 Persson, Ch., Wern, L. (1985)
Spridnings- och depositionsberäkningar för avfallsförbränningsanläggning i Sofielund.
- 13 Persson, Ch., Wern, L. (1985)
Spridnings- och depositionsberäkningar för avfallsförbränningsanläggning i Högdalen.
- 14 Vedin, H., Andersson, C. (1985)
Extrema köldperioder i Stockholm.
- 15 Krieg, R., Omstedt, G. (1985)
Spridningsberäkningar för Volvos planerade bilfabrik i Uddevalla.
- 16 Kindell, S., Wern, L. (1985)
Luftvårdsstudie avseende industrikombinatet i Nynäshamn (koncentrations- och luktberäkningar).
- 17 Laurin, S., Persson, Ch. (1985)
Beräknad formaldehydspridning och deposition från SWEDSPANs spånskivefabrik.
- 18 Persson, Ch., Wern, L. (1985)
Luftvårdsstudie avseende industrikombinatet i Nynäshamn – depositionsberäkningar av koldamm.

- 19 Fredriksson, U. (1985)
Luktberäkningar för Bofors Plast i Ljungby, II.
- 20 Wern, L., Omstedt, G. (1985)
Spridningsberäkningar för Volvos planerade bilfabrik i Uddevalla - energicentralen.
- 21 Krieg, R., Omstedt, G. (1985)
Spridningsberäkningar för Volvos planerade bilfabrik i Uddevalla - kompletterande beräkningar för fabrikena.
- 22 Karlsson, K.-G. (1985)
Information från Meteosat - forskningsrön och operationell tillämpning.
- 23 Fredriksson, U. (1985)
Spridningsberäkningar för AB Åkerlund & Rausings fabrik i Lund.
- 24 Färnlöf, S. (1985)
Radarmeteorologi.
- 25 Ahlström, B., Salomonsson, G. (1985)
Resultat av 5-dygnsprognois till ledning för isbrytarverksamhet vintern 1984-85.
- 26 Wern, L. (1985)
Avesta stadsmodell.
- 27 Hultberg, H. (1985)
Statistisk prognos av ytttemperatur.
- 1986
- 1 Krieg, R., Johansson, L., Andersson, C. (1986)
Vindmätningar i höga master, kvartalsrapport 3/1985.
- 2 Olsson, L.-E., Kindell, S. (1986)
Air pollution impact assessment for the SABAH timber, pulp and paper complex.
- 3 Ivarsson, K.-I. (1986)
Resultat av byggväderprognoser - säsongen 1984/85.
- 4 Persson, Ch., Robertson, L. (1986)
Spridnings- och depositionsberäkningar för en sopförbränningsanläggning i Skövde.
- 5 Laurin, S. (1986)
Bilavgaser vid intagsplan - Eskilstuna.
- 6 Robertson, L. (1986)
Koncentrations- och depositionsberäkningar för en sopförbränningsanläggning vid Ryaverken i Borås.
- 7 Laurin, S. (1986)
Luften i Avesta - föroreningsbidrag från trafiken.
- 8 Robertson, L., Ring, S. (1986)
Spridningsberäkningar för bromcyan.
- 9 Wern, L. (1986)
Extrema byvindar i Orrefors.
- 10 Robertson, L. (1986)
Koncentrations- och depositionsberäkningar för Halmstads avfallsförbränningsanläggning vid Kristinehed.
- 11 Törnevik, H., Ugnell (1986)
Belastningsprognoser.
- 12 Joelsson, R. (1986)
Något om användningen av numeriska prognoser på SMHI (i princip rapporten till ECMWF).
- 13 Krieg, R., Andersson, C. (1986)
Vindmätningar i höga master, kvartalsrapport 4/1985.
- 14 Dahlgren, L. (1986)
Solmätning vid SMHI.
- 15 Wern, L. (1986)
Spridningsberäkningar för ett kraftvärmeverk i Sundbyberg.
- 16 Kindell, S. (1986)
Spridningsberäkningar för Uddevallas fjärrvärmecentral i Hovhult.
- 17 Häggkvist, K., Persson, Ch., Robertson, L. (1986)
Spridningsberäkningar rörande gasutsläpp från ett antal källor inom SSAB Luleå-verken.
- 18 Krieg, R., Wern, L. (1986)
En klimatstudie för Arlanda stad.
- 19 Vedin, H. (1986)
Extrem arealnederbörd i Sverige.
- 20 Wern, L. (1986)
Spridningsberäkningar för lösningsmedel i Tibro.
- 21 Krieg, R., Andersson, C. (1986)
Vindmätningar i höga master - kvartalsrapport 1/1986.

- 22 Kvick, T. (1986)
Beräkning av vindenergitillgången på några platser i Halland och Bohuslän.
- 23 Krieg, R., Andersson, C. (1986)
Vindmätningar i höga master - kvartalsrapport 2/1986.
- 24 Persson, Ch. (SMHI), Rodhe, H. (MISU), De Geer, L.-E. (FOA) (1986)
Tjernobylolyckan - En meteorologisk analys av hur radioaktivitet spreds till Sverige.
- 25 Fredriksson, U. (1986)
Spridningsberäkningar för Spendrups bryggeri, Grängesberg.
- 26 Krieg, R. (1986)
Beräkningar av vindenergitillgången på några platser i Skåne.
- 27 Wern, L., Ring, S. (1986)
Spridningsberäkningar, SSAB.
- 28 Wern, L., Ring, S. (1986)
Spridningsberäkningar för ny ugn, SSAB II.
- 29 Wern, L. (1986)
Spridningsberäkningar för Volvo Hallsbergverken.
- 30 Fredriksson, U. (1986)
SO₂-halter från Hammarbyverket kring ny arena vid Johanneshov.
- 31 Persson, Ch., Robertson, L., Häggkvist, K. (1986)
Spridningsberäkningar, SSAB - Luleåverken.
- 32 Kindell, S., Ring, S. (1986)
Spridningsberäkningar för SAABs planerade bilfabrik i Malmö.
- 33 Wern, L. (1986)
Spridningsberäkningar för svavelsyrafabrik i Falun.
- 34 Wern, L., Ring, S. (1986)
Spridningsberäkningar för Västhamnsverket HKV1 i Helsingborg.
- 35 Persson, Ch., Wern, L. (1986)
Beräkningar av svaveldepositionen i Stockholmsområdet.
- 36 Joelsson, R. (1986)
USAs månadsprognoser.
- 37 Vakant nr.
- 38 Krieg, R., Andersson, C. (1986)
Utemiljön vid Kvarnberget, Lysekil.
- 39 Häggkvist, K. (1986)
Spridningsberäkningar av freon 22 från Ropstens värmepumpverk.
- 40 Fredriksson, U. (1986)
Vindklassificering av en plats på Hemsön.
- 41 Nilsson, S. (1986)
Utvärdering av sommarens (1986) använda konvektionsprognoshjälpmedel.
- 42 Krieg, R., Kvick, T. (1986)
Vindmätningar i höga master.
- 43 Krieg, R., Fredriksson, U. (1986)
Vindarna över Sverige.
- 44 Robertson, L. (1986)
Spridningsberäkningar rörande gasutsläpp vid ScanDust i Landskrona - bestämning av cyanvätehalter.
- 45 Kvick, T., Krieg, R., Robertson, L. (1986)
Vindförhållandena i Sveriges kust- och havsband, rapport nr 2.
- 46 Fredriksson, U. (1986)
Spridningsberäkningar för en planerad panncentral vid Lindsdal utanför Kalmar.
- 47 Fredriksson, U. (1986)
Spridningsberäkningar för Volvo BMs fabrik i Landskrona.
- 48 Fredriksson, U. (1986)
Spridningsberäkningar för ELMO-CALFs fabrik i Svenljunga.
- 49 Häggkvist, K. (1986)
Spridningsberäkningar rörande gasutsläpp från syrgas- och bensenupplag inom SSAB Luleåverken.
- 50 Wern, L., Fredriksson, U., Ring, S. (1986)
Spridningsberäkningar för lösningsmedel i Tidaholm.
- 51 Wern, L. (1986)
Spridningsberäkningar för Volvo BM ABs anläggning i Braås.

- 22 Kwick, T. (1986)
Beräkning av vindenergitillgången på några platser i Halland och Bohuslän.
- 23 Krieg, R., Andersson, C. (1986)
Vindmätningar i höga master - kvartalsrapport 2/1986.
- 24 Persson, Ch. (SMHI), Rodhe, H. (MISU), De Geer, L.-E. (FOA) (1986)
Tjernobylylyckan - En meteorologisk analys av hur radioaktivitet spreds till Sverige.
- 25 Fredriksson, U. (1986)
Spridningsberäkningar för Spendrups bryggeri, Grängesberg.
- 26 Krieg, R. (1986)
Beräkningar av vindenergitillgången på några platser i Skåne.
- 27 Wern, L., Ring, S. (1986)
Spridningsberäkningar, SSAB.
- 28 Wern, L., Ring, S. (1986)
Spridningsberäkningar för ny ugn, SSAB II.
- 29 Wern, L. (1986)
Spridningsberäkningar för Volvo Hallsbergverken.
- 30 Fredriksson, U. (1986)
SO₂-halter från Hammarbyverket kring ny arena vid Johanneshov.
- 31 Persson, Ch., Robertson, L., Häggkvist, K. (1986)
Spridningsberäkningar, SSAB - Luleåverken.
- 32 Kindell, S., Ring, S. (1986)
Spridningsberäkningar för SAABs planerade bilfabrik i Malmö.
- 33 Wern, L. (1986)
Spridningsberäkningar för svavelsyrafabrik i Falun.
- 34 Wern, L., Ring, S. (1986)
Spridningsberäkningar för Västhamnsverket HKV1 i Helsingborg.
- 35 Persson, Ch., Wern, L. (1986)
Beräkningar av svaveldepositionen i Stockholmsområdet.
- 36 Joelsson, R. (1986)
USAs månadsprognoser.
- 37 Vakant nr.
- 38 Krieg, R., Andersson, C. (1986)
Utemiljön vid Kvarnberget, Lysekil.
- 39 Häggkvist, K. (1986)
Spridningsberäkningar av freon 22 från Ropstens värmepumpverk.
- 40 Fredriksson, U. (1986)
Vindklassificering av en plats på Hemsön.
- 41 Nilsson, S. (1986)
Utvärdering av sommarens (1986) använda konvektionsprognoshjälpmedel.
- 42 Krieg, R., Kwick, T. (1986)
Vindmätningar i höga master.
- 43 Krieg, R., Fredriksson, U. (1986)
Vindarna över Sverige.
- 44 Robertson, L. (1986)
Spridningsberäkningar rörande gasutsläpp vid ScanDust i Landskrona - bestämning av cyanvätehalter.
- 45 Kwick, T., Krieg, R., Robertson, L. (1986)
Vindförhållandena i Sveriges kust- och havsband, rapport nr 2.
- 46 Fredriksson, U. (1986)
Spridningsberäkningar för en planerad panncentral vid Lindsdal utanför Kalmar.
- 47 Fredriksson, U. (1986)
Spridningsberäkningar för Volvo BMs fabrik i Landskrona.
- 48 Fredriksson, U. (1986)
Spridningsberäkningar för ELMO-CALFs fabrik i Svenljunga.
- 49 Häggkvist, K. (1986)
Spridningsberäkningar rörande gasutsläpp från syrgas- och bensenupplag inom SSAB Luleåverken.
- 50 Wern, L., Fredriksson, U., Ring, S. (1986)
Spridningsberäkningar för lösningsmedel i Tidaholm.
- 51 Wern, L. (1986)
Spridningsberäkningar för Volvo BM ABs anläggning i Braås.

- 52 Ericson, K. (1986)
Meteorological measurements performed May 15, 1984, to June, 1984, by the SMHI.
- 53 Wern, L., Fredriksson, U. (1986)
Spridningsberäkning för Kockums Plåtteknik, Ronneby.
- 54 Eriksson, B. (1986)
Frekvensanalys av timvisa temperatur-observationer.
- 55 Wern, L., Kindell, S. (1986)
Luktberäkningar för AB ELMO i Flen.
- 56 Robertson, L. (1986)
Spridningsberäkningar rörande utsläpp av NO_x inom Fagersta kommun.
- 57 Kindell, S. (1987)
Luften i Nässjö.
- 58 Persson, Ch., Robertson, L. (1987)
Spridningsberäkningar rörande gasutsläpp vid ScanDust i Landskrona - bestämning av cyanväte.
- 59 Bringfelt, B. (1987)
Receptorbaserad partikelmodell för gatumiljömodell för en gata i Nyköping.
- 60 Robertson, L. (1987)
Spridningsberäkningar för Varbergs kommun. Bestämning av halter av SO₂, CO, NO_x samt några kolväten.
- 61 Vedin, H., Andersson, C. (1987)
E 66 - Linderödsåsen - klimatförhållanden.
- 62 Wern, L., Fredriksson, U. (1987)
Spridningsberäkningar för Kockums Plåtteknik, Ronneby. 2.
- 63 Taesler, R., Andersson, C., Wallentin, C., Krieg, R. (1987)
Klimatkorrigering för energiförbrukningen i ett eluppvärmt villaområde.
- 64 Fredriksson, U. (1987)
Spridningsberäkningar för AB Åetå-Trycks planerade anläggning vid Kungens Kurva.
- 65 Melgarejo, J. (1987)
Mesoskalig modellering vid SMHI.
- 66 Häggkvist, K. (1987)
Vindlaster på kordahus vid Alviks Strand - numeriska beräkningar.
- 67 Persson, Ch. (1987)
Beräkning av lukt och föroreningshalter i luft runt Neste Polyester i Nol.
- 68 Fredriksson, U., Krieg, R. (1987)
En överskalig klimatstudie för Tornby, Linköping.
- 69 Häggkvist, K. (1987)
En numerisk modell för beräkning av vertikal momentumtransport i områden med stora råhetelement. Tillämpning på ett energiskogsområde.
- 70 Lindström, Kjell (1987)
Weather and flying briefing aspects.
- 71 Häggkvist, K. (1987)
En numerisk modell för beräkning av vertikal momentumtransport i områden med stora råhetelement. En koefficientbestämning.
- 72 Liljas, E. (1988)
Förbättrad väderinformation i jordbruket - behov och möjligheter (PROFARM).
- 73 Andersson, Tage (1988)
Isbildning på flygplan.
- 74 Andersson, Tage (1988)
Aeronautic wind shear and turbulence. A review for forecasts.
- 75 Källberg, P. (1988)
Parameterisering av diabatiska processer i numeriska prognosmodeller.
- 76 Vedin, H., Eriksson, B. (1988)
Extrem arealnederbörd i Sverige 1881 - 1988.
- 77 Eriksson, B., Carlsson, B., Dahlström, B. (1989)
Preliminär handledning för korrektion av nederbördsmängder.
- 78 Liljas, E. (1989)
Torv-väder. Behovsanalys med avseende på väderprognoser och produktion av bränsletorv.
- 79 Hagmarker, A. (1991)
Satellitmeteorologi.
- 80 Lövblad, G., Persson, Ch. (1991)
Background report on air pollution situation in the Baltic states - a prefeasibility study.
IVL Publikation B 1038.

- 81 Alexandersson, H., Karlström, C., Larsson-McCann, S. (1991)
Temperaturen och nederbörden i Sverige 1961-90. Referensnormaler.
- 82 Vedin, H., Alexandersson, H., Persson, M. (1991)
Utnyttjande av persistens i temperatur och nederbörd för vårflödesprognoser.
- 83 Moberg, A. (1992)
Lufttemperaturen i Stockholm 1756 - 1990. Historik, inhomogeniteter och urbaniseringseffekt. Naturgeografiska Institutionen, Stockholms Universitet.
- 84 Josefsson, W. (1993)
Normalvärden för perioden 1961-90 av globalstrålning och solskenstid i Sverige.
- 85 Laurin, S., Alexandersson, H. (1994)
Några huvuddrag i det svenska temperatur-klimatet 1961 - 1990.
- 86 Fredriksson, U. och Ståhl, S. (1994)
En jämförelse mellan automatiska och manuella fältmätningar av temperatur och nederbörd.
- 87 Alexandersson, H., Eggertsson Karlström, C. och Laurin S. (1997).
Några huvuddrag i det svenska nederbördsklimatet 1961-1990.
- 88 Mattsson, J., Rummukainen, M. (1998)
Växthuseffekten och klimatet i Norden - en översikt.
- 89 Kindbom, K., Sjöberg, K., Munthe, J., Peterson, K. (IVL) Persson, C. Roos, E., Bergström, R. (SMHI). (1998)
Nationell miljöövervakning av luft- och nederbördskemi 1996.
- 90 Foltescu, V.L., Häggmark, L (1998)
Jämförelse mellan observationer och fält med griddad klimatologisk information.
- 91 Hultgren, P., Dybbroe, Karlsson, K.-G. (1999)
SCANDIA – its accuracy in classifying LOW CLOUDS
- 92 Hyvarinen, O., Karlsson, K.-G., Dybbroe, A. (1999)
Investigations of NOAA AVHRR/3 1.6 μm imagery for snow, cloud and sunglint discrimination (Nowcasting SAF)
- 93 Bennartz, R., Thoss, A., Dybbroe, A. and Michelson, D. B. (1999)
Precipitation Analysis from AMSU (Nowcasting SAF)
- 94 Appelqvist, Peter och Anders Karlsson (1999)
Nationell emissionsdatabas för utsläpp till luft - Förstudie.
- 95 Persson, C., Robertson L. (SMHI) Thaning, L (LFOA). (2000)
Model for Simulation of Air and Ground Contamination Associated with Nuclear Weapons. An Emergency Preparedness Model.
- 96 Kindbom K., Svensson A., Sjöberg K., (IVL) Persson C., (SMHI) (2001)
Nationell miljöövervakning av luft- och nederbördskemi 1997, 1998 och 1999.
- 97 Diamandi, A., Dybbroe, A. (2001)
Nowcasting SAF
Validation of AVHRR cloud products.
- 98 Foltescu V. L., Persson C. (2001)
Beräkningar av moln- och dimdeposition i Sverigemodellen - Resultat för 1997 och 1998.
- 99 Alexandersson, H. och Eggertsson Karlström, C (2001)
Temperaturen och nederbörden i Sverige 1961-1990. Referensnormaler - utgåva 2.
- 101 Josefsson, W. (1989)
Computed global radiation using interpolated, gridded cloudiness from the MESA-BETA analysis compared to measured global radiation.

- 22 Kwick, T. (1986)
Beräkning av vindenergitillgången på några platser i Halland och Bohuslän.
- 23 Krieg, R., Andersson, C. (1986)
Vindmätningar i höga master - kvartalsrapport 2/1986.
- 24 Persson, Ch. (SMHI), Rodhe, H. (MISU), De Geer, L.-E. (FOA) (1986)
Tjernobylyolyckan - En meteorologisk analys av hur radioaktivitet spreds till Sverige.
- 25 Fredriksson, U. (1986)
Spridningsberäkningar för Spendrups bryggeri, Grängesberg.
- 26 Krieg, R. (1986)
Beräkningar av vindenergitillgången på några platser i Skåne.
- 27 Wern, L., Ring, S. (1986)
Spridningsberäkningar, SSAB.
- 28 Wern, L., Ring, S. (1986)
Spridningsberäkningar för ny ugn, SSAB II.
- 29 Wern, L. (1986)
Spridningsberäkningar för Volvo Hallsbergverken.
- 30 Fredriksson, U. (1986)
SO₂-halter från Hammarbyverket kring ny arena vid Johanneshov.
- 31 Persson, Ch., Robertson, L., Häggkvist, K. (1986)
Spridningsberäkningar, SSAB - Luleåverken.
- 32 Kindell, S., Ring, S. (1986)
Spridningsberäkningar för SAABs planerade bilfabrik i Malmö.
- 33 Wern, L. (1986)
Spridningsberäkningar för svavelsyrafabrik i Falun.
- 34 Wern, L., Ring, S. (1986)
Spridningsberäkningar för Västhamnsverket HKV1 i Helsingborg.
- 35 Persson, Ch., Wern, L. (1986)
Beräkningar av svaveldepositionen i Stockholmsområdet.
- 36 Joelsson, R. (1986)
USAs månadsprognoser.
- 37 Vakant nr.
- 38 Krieg, R., Andersson, C. (1986)
Utemiljön vid Kvarnberget, Lysekil.
- 39 Häggkvist, K. (1986)
Spridningsberäkningar av freon 22 från Ropstens värmepumpverk.
- 40 Fredriksson, U. (1986)
Vindklassificering av en plats på Hemsön.
- 41 Nilsson, S. (1986)
Utvärdering av sommarens (1986) använda konvektionsprognoshjälpmedel.
- 42 Krieg, R., Kwick, T. (1986)
Vindmätningar i höga master.
- 43 Krieg, R., Fredriksson, U. (1986)
Vindarna över Sverige.
- 44 Robertson, L. (1986)
Spridningsberäkningar rörande gasutsläpp vid ScanDust i Landskrona - bestämning av cyanvätehalter.
- 45 Kwick, T., Krieg, R., Robertson, L. (1986)
Vindförhållandena i Sveriges kust- och havsband, rapport nr 2.
- 46 Fredriksson, U. (1986)
Spridningsberäkningar för en planerad panncentral vid Lindsdal utanför Kalmar.
- 47 Fredriksson, U. (1986)
Spridningsberäkningar för Volvo BMs fabrik i Landskrona.
- 48 Fredriksson, U. (1986)
Spridningsberäkningar för ELMO-CALFs fabrik i Svenljunga.
- 49 Häggkvist, K. (1986)
Spridningsberäkningar rörande gasutsläpp från syrgas- och bensenupplag inom SSAB Luleåverken.
- 50 Wern, L., Fredriksson, U., Ring, S. (1986)
Spridningsberäkningar för lösningsmedel i Tidaholm.
- 51 Wern, L. (1986)
Spridningsberäkningar för Volvo BM ABs anläggning i Braås.



Sveriges meteorologiska och hydrologiska institut
601 76 Norrköping · Tel 011-495 8000 · Fax 011-495 8001
www.smhi.se

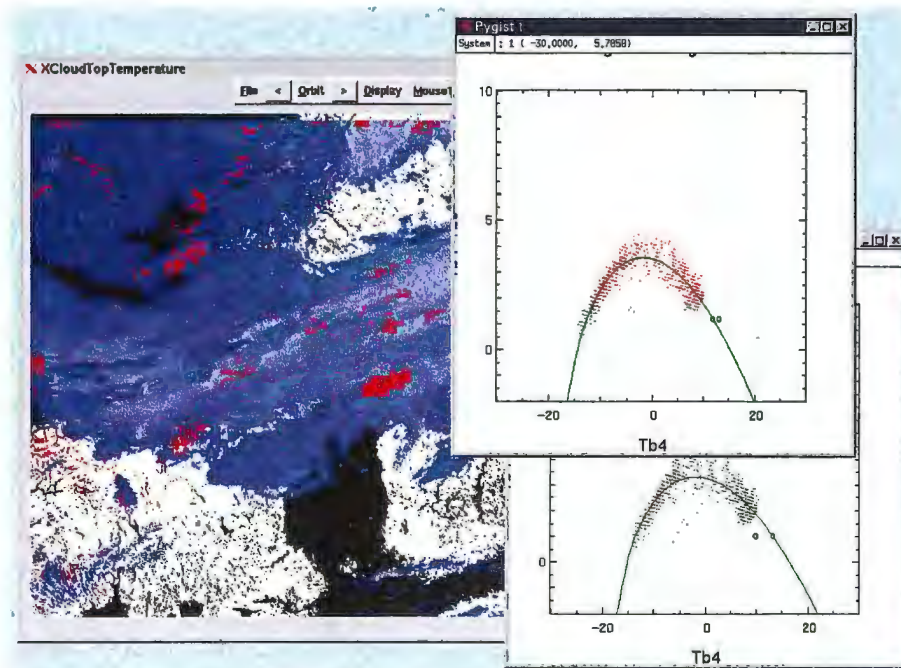


Figure 4: GUI display of the model fit for a requested segment.

taining AAPP processing results for HIRS data. After computing the radiance ratio estimate for each HIRS fov it then compares these results against the nearest histogram method results. The program reports the bias and standard deviation for the two methods.

background is opaque cloud at the lower level. Finally the inside region of the distribution is formed when the two cloud layers both are transparent in various degree.

The model fit tries to compromise between the three arcs, and inevitably fails to retrieve either of the two cloud temperatures correctly. The resulting cloud top temperature is too cold and is rejected by applying quality control checks. In this case the rmse of the distribution is 0.704 K against the assumed model, so that a limit 0.7 for the rmse would correctly reject the result, but a safer limit below 0.7 is suggested by this example. With a more sophisticated histogram analysis the two cloud layer temperatures could be retrieved, but even then it would be difficult to assign the temperature and height to the semi-transparent pixels because the three distributions overlap.

In the case when there is a lower level opaque cloud filling the segment, and a semi-transparent layer above, the histogram method can still retrieve the upper level temperature. The parameters T_s and δ_s have non-relevant (cloud-clear surface) first guess values for the case, but during the least-squares fitting they can still become adjusted to the opaque cloud values.

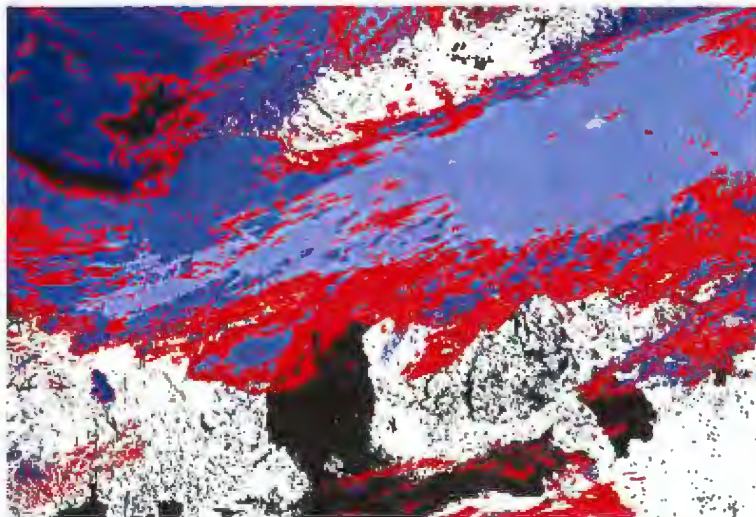


Figure 6: NOAA14 satellite pass at 24-Sep-2000 1434 UTC. Cloud top temperature in opaque cloud pixels, determined from uncorrected AVHRR radiances, are shown in blue colours. The remaining cloudy pixels, which require the correction are shown in red.

To give an example of the overall performance we show here the resulting cloud top temperature images when we apply the histogram method to the case shown in the cover image, or again in figure 6. Of the target pixels shown in red 91% in this particular case were classified as semi-transparent, and 9% as fractional. For the two test runs we set the rmse quality control threshold to 0.7 In the first testrun we used only the fixed image segmenta-

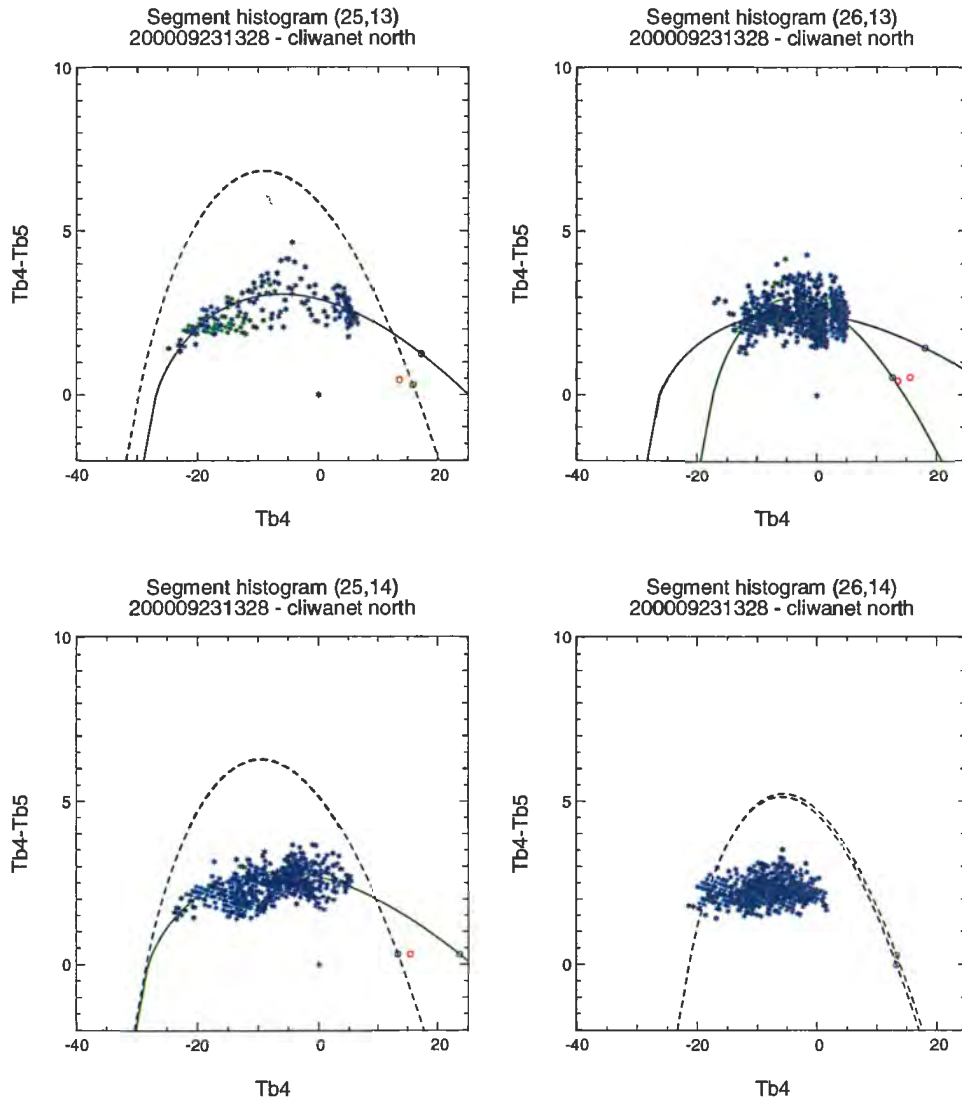


Figure 14: Histogram and fitted curves for the four segments corresponding to the 1st and 2nd column and the 1st and 2nd row (in segment resolution counted from upper left corner) of the close-up shown in figure 13. The segment numbers of the original cliwanet north area of the NOAA 12 scene 13:28 UTC September 23, 2000, are written above the plots. See capt of figure 11 for further explanations.



Sveriges meteorologiska och hydrologiska institut
601 76 Norrköping · Tel 011-495 8000 · Fax 011-495 8001
www.smhi.se

From the satellite data at 13:08 UTC we get cloud top heights of 2600m to 3400m in and a little to the north of the marked area, and for the higher cloud deck a little to the south west, referred to, we get cloud top heights of 4800m to 5800m (the green colours in the right panel of figure 16).

Later at 14:47 UTC we get cloud top heights between 2200m and 3200m for the lower cloud deck and approximately 4200m to 5200m for the higher one. The high clouds look more fuzzy and less opaque in the RGB images at this time, indicating that the clouds may be in the process of dissolving. To the north of the area there are several clearly detectable patches of low level clouds which from the cloud top temperature image look rather homogeneous. These clouds have tops around 2600m to 3400m, thus a little higher than what was retrieved closer to the observation point.

Though the above clearly demonstrate the limitations in this kind of intercomparison we can conclude that the satellite retrieval does not contradict the aircraft observations. But as observed in the figures 16 and 17 most clouds are detected as opaque, and therefore a direct validation of the semi-transparent retrieval is not possible. The semi-transparent retrieval proved to be able to add only little extra information here.

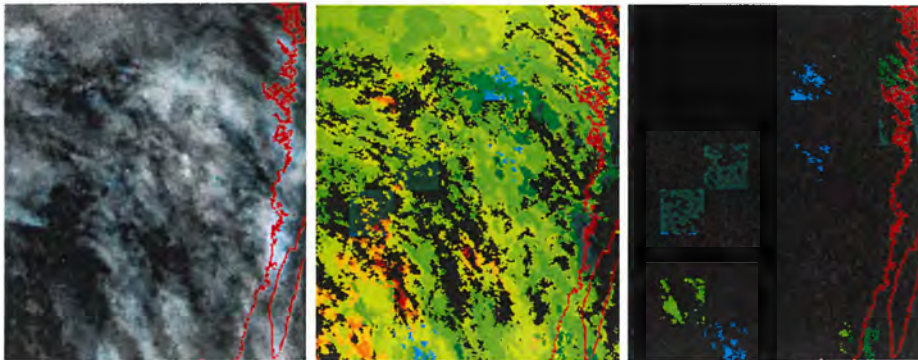


Figure 17: Channel 3,4,5 RGB image (left panel) and cloud top height using both the opaque and semi-transparent retrievals (middle) and the semi-transparent only (right) of a NOAA 14 pass on November 9, 2000, 14:47 UTC. Close-up on the area around and south of the lake Sommen in southern Sweden, where the two cloud top observations were made.

Having verified that the cloud top height of the opaque retrieval fits the observations rather well, one could check nearby areas with results from both the opaque and the semi-transparent retrievals, in order to make an indirect validation of the latter. The two closest segments with some results of the semi-transparent retrieval are found on the border of the higher cloud and the lower cloud just to the east of where we have the cloud top observation of the low cloud, and two segments further to the south (the two segments with cyan colours in the upper part of the image shown in the right panel of figure 17).

The histograms of these two segments are shown in figure 18. In both cases the curve fit is rather good on the land pixels, but the low number of points in the histogram illustrate well the shortcomings of the method in this case. From the points alone it is impossible to see a curved pattern in the histogram. At the northern most segment, on the edge of the higher cloud, the result agrees very well with the opaque retrieval, giving a height of $4200m$ and a temperature of $254K$. The segment to the south give cloud top heights of around $7400m$, or approximately $2000m$ above what is found with the opaque retrieval.

- 52 Ericson, K. (1986)
Meteorological measurements performed May 15, 1984, to June, 1984, by the SMHI.
- 53 Wern, L., Fredriksson, U. (1986)
Spridningsberäkning för Kockums Plåtteknik, Ronneby.
- 54 Eriksson, B. (1986)
Frekvensanalys av timvisa temperaturobservationer.
- 55 Wern, L., Kindell, S. (1986)
Luktberäkningar för AB ELMO i Flen.
- 56 Robertson, L. (1986)
Spridningsberäkningar rörande utsläpp av NO_x inom Fagersta kommun.
- 57 Kindell, S. (1987)
Luften i Nässjö.
- 58 Persson, Ch., Robertson, L. (1987)
Spridningsberäkningar rörande gasutsläpp vid ScanDust i Landskrona - bestämning av cyanväte.
- 59 Bringfelt, B. (1987)
Receptorbaserad partikelmodell för gatumiljömodell för en gata i Nyköping.
- 60 Robertson, L. (1987)
Spridningsberäkningar för Varbergs kommun. Bestämning av halter av SO₂, CO, NO_x samt några kolväten.
- 61 Vedin, H., Andersson, C. (1987)
E 66 - Linderödsåsen - klimatförhållanden.
- 62 Wern, L., Fredriksson, U. (1987)
Spridningsberäkningar för Kockums Plåtteknik, Ronneby. 2.
- 63 Taesler, R., Andersson, C., Wallentin, C., Krieg, R. (1987)
Klimatkorrigering för energiförbrukningen i ett eluppvärmt villaområde.
- 64 Fredriksson, U. (1987)
Spridningsberäkningar för AB Åetå-Trycks planerade anläggning vid Kungens Kurva.
- 65 Melgarejo, J. (1987)
Mesoskalig modellering vid SMHI.
- 66 Häggkvist, K. (1987)
Vindlaster på kordahus vid Alviks Strand - numeriska beräkningar.
- 67 Persson, Ch. (1987)
Beräkning av lukt och föroreningshalter i luft runt Neste Polyester i Nol.
- 68 Fredriksson, U., Krieg, R. (1987)
En överskalig klimatstudie för Tornby, Linköping.
- 69 Häggkvist, K. (1987)
En numerisk modell för beräkning av vertikal momentumtransport i områden med stora råhetselement. Tillämpning på ett energiskogsområde.
- 70 Lindström, Kjell (1987)
Weather and flying briefing aspects.
- 71 Häggkvist, K. (1987)
En numerisk modell för beräkning av vertikal momentumtransport i områden med stora råhetselement. En koefficientbestämning.
- 72 Liljas, E. (1988)
Förbättrad väderinformation i jordbruket - behov och möjligheter (PROFARM).
- 73 Andersson, Tage (1988)
Isbildning på flygplan.
- 74 Andersson, Tage (1988)
Aeronautic wind shear and turbulence. A review for forecasts.
- 75 Källberg, P. (1988)
Parameterisering av diabatiska processer i numeriska prognosmodeller.
- 76 Vedin, H., Eriksson, B. (1988)
Extrem arealnederbörd i Sverige 1881 - 1988.
- 77 Eriksson, B., Carlsson, B., Dahlström, B. (1989)
Preliminär handledning för korrektion av nederbördsmängder.
- 78 Liljas, E. (1989)
Torv-väder. Behovsanalys med avseende på väderprognoser och produktion av bränsletorv.
- 79 Hagmarker, A. (1991)
Satellitmeteorologi.
- 80 Lövblad, G., Persson, Ch. (1991)
Background report on air pollution situation in the Baltic states - a prefeasibility study.
IVL Publikation B 1038.

- 81 Alexandersson, H., Karlström, C., Larsson-McCann, S. (1991)
Temperaturen och nederbörden i Sverige 1961-90. Referensnormaler.
- 82 Vedin, H., Alexandersson, H., Persson, M. (1991)
Utnyttjande av persistens i temperatur och nederbörd för vårflödesprognoser.
- 83 Moberg, A. (1992)
Lufttemperaturen i Stockholm 1756 - 1990. Historik, inhomogeniteter och urbaniseringseffekt. Naturgeografiska Institutionen, Stockholms Universitet.
- 84 Josefsson, W. (1993)
Normalvärden för perioden 1961-90 av globalstrålning och solskenstid i Sverige.
- 85 Laurin, S., Alexandersson, H. (1994)
Några huvuddrag i det svenska temperatur-klimatet 1961 - 1990.
- 86 Fredriksson, U. och Ståhl, S. (1994)
En jämförelse mellan automatiska och manuella fältmätningar av temperatur och nederbörd.
- 87 Alexandersson, H., Eggertsson Karlström, C. och Laurin S. (1997).
Några huvuddrag i det svenska nederbördsklimatet 1961-1990.
- 88 Mattsson, J., Rummukainen, M. (1998)
Växthuseffekten och klimatet i Norden - en översikt.
- 89 Kindbom, K., Sjöberg, K., Munthe, J., Peterson, K. (IVL) Persson, C. Roos, E., Bergström, R. (SMHI). (1998)
Nationell miljöövervakning av luft- och nederbördskemi 1996.
- 90 Foltescu, V.L., Häggmark, L (1998)
Jämförelse mellan observationer och fält med griddad klimatologisk information.
- 91 Hultgren, P., Dybbroe, Karlsson, K.-G. (1999)
SCANDIA – its accuracy in classifying LOW CLOUDS
- 92 Hyvarinen, O., Karlsson, K.-G., Dybbroe, A. (1999)
Investigations of NOAA AVHRR/3 1.6 μm imagery for snow, cloud and sunglint discrimination (Nowcasting SAF)
- 93 Bennartz, R., Thoss, A., Dybbroe, A. and Michelson, D. B. (1999)
Precipitation Analysis from AMSU (Nowcasting SAF)
- 94 Appelqvist, Peter och Anders Karlsson (1999)
Nationell emissionsdatabas för utsläpp till luft - Förstudie.
- 95 Persson, C., Robertson L. (SMHI) Thaning, L (LFOA). (2000)
Model for Simulation of Air and Ground Contamination Associated with Nuclear Weapons. An Emergency Preparedness Model.
- 96 Kindbom K., Svensson A., Sjöberg K., (IVL) Persson C., (SMHI) (2001)
Nationell miljöövervakning av luft- och nederbördskemi 1997, 1998 och 1999.
- 97 Diamandi, A., Dybbroe, A. (2001)
Nowcasting SAF
Validation of AVHRR cloud products.
- 98 Foltescu V. L., Persson C. (2001)
Beräkningar av moln- och dimdeposition i Sverigemodellen - Resultat för 1997 och 1998.
- 99 Alexandersson, H. och Eggertsson Karlström, C (2001)
Temperaturen och nederbörden i Sverige 1961-1990. Referensnormaler - utgåva 2.
- 101 Josefsson, W. (1989)
Computed global radiation using interpolated, gridded cloudiness from the MESA-BETA analysis compared to measured global radiation.



Sveriges meteorologiska och hydrologiska institut
601 76 Norrköping · Tel 011-495 8000 · Fax 011-495 8001
www.smhi.se